XI. PLASMA ELECTRONICS*

Prof. H. A. Haus
Prof. A. Bers
Prof. W. D. Getty
Prof. G. D. Bernard
Prof. D. J. Rose
Prof. T. H. Dupree
Prof. L. M. Lidsky
Prof. E. P. Gyftopoulos
Dr. T. Musha
R. R. Bartsch
T. S. Brown
J. F. Clarke
D. E. Crane
J. A. Davis
R. W. Flynn
J. N. Hamawi
W. T. Hebel, Jr.
C-F. G. Hsi
B. R. Kusse
S. H. Kyong
M. A. Lieberman
M. D. Lubin
R. W. Moir
A. A. Offenberger
R. R. Parker
C. S. Ribbeck
E. A. Robertson
M. A. Samis
H. M. Schneider
C. E. Speck
C. E. Wagner
R. N. Wallace
J. C. Woo
N. D. Woodson

A. ACTIVE SOLID-STATE PLASMAS

1. STIMULATED EMISSION OF PHONONS BY ELECTRONS DRIFTING ALONG THE MAGNETIC FIELD

In this report we present the results of a quantum-mechanical analysis of the interaction between acoustic phonons and electrons drifting along an external magnetic field, and show the possible relation to recent experiments.[1,2] The coupling between the electrons and phonons is taken through the deformation potential. We find that stimulated emission of phonons, with electrons making transitions between Landau levels, has a threshold magnetic field.

We neglect electron-electron interactions, which is valid for high-frequency phonons in semiconductors ($q\ell_s \gg 1$, where q is the phonon wave number, and ℓ_s is the screening length for the electrons). The interaction Hamiltonian for the deformation potential in terms of electron and phonon operators is $H' = \int \Psi^+ C\Delta(x)\, \Psi\, d^3x$, where Ψ is the field operator for electrons in the Landau gauge,[3] Δ is the dilation,[4] and C is the deformation potential coefficient. Assuming that the gyration radius of the electron is small compared with the phonon wavelength (dipole approximation), we expand H' up to first order in $\vec{q} \cdot \vec{x}$ and obtain

$$
\begin{aligned}
H' = & \sum_{\vec{q}, n, \vec{k}} iC(\hbar/2\rho V\omega_q)^{1/2}\, q\xi_n c^+_{\vec{k}+\vec{q}, n}\, c_{\vec{k}, n}\left(a_{\vec{q}} - a^+_{-\vec{q}}\right) \\
& - \sum_{\vec{q}, n, \vec{k}} \Bigg\{ iC(\hbar/2\rho V\omega_q)^{1/2}\, q(\hbar/2m\omega_c)^{1/2}\, qx \\
& \times \left[n^{1/2}\xi_{n-1} c^+_{\vec{k}+\vec{q}, n-1} - (n+1)^{1/2}\xi_{n+1} c^+_{\vec{k}+\vec{q}, n+1} \right] c_{\vec{k}, n}\left(a_{\vec{q}} - a^+_{-\vec{q}}\right) \Bigg\} \qquad (1)
\end{aligned}
$$

---

*The work reported in Sections XI-A, -B, -C, and -D was supported principally by the National Science Foundation (Grant GK-524).

where ρ is the mass density; V, the volume; ω_q, the angular frequency of the phonon with wave number $\vec{q}$; $a_{\vec{q}}$ and $a^+_{\vec{q}}$, the phonon operators; $c_{\vec{k},n} = c(k_y, k_z, n)$ and $c^+_{\vec{k},n}$, the electron Fermi operators; m, the effective mass which has been set equal to the electron cyclotron mass; and $\omega_c = eB_o/m$, the electron cyclotron frequency. In (1) ξ_n is given by

$$\xi_n(q_y) = \int \eta_n(x)\, \eta(x-\hbar q_y/m\omega_c)\, dx \tag{2}$$

and represents an overlap integral of two harmonic oscillator states in the interaction. These two states have different equilibrium positions, separated by $\delta = \hbar q_y/m\omega_c$ caused by the recoil of emitted or absorbed phonons. The overlap integral (2) becomes very small if the separation is larger than the first zero of the harmonic oscillator function[5] given by $F_n(\hbar/m\omega_c)^{1/2}$, where F_n is approximately unity. Hence, in order to get appreciable interaction we require

$$B_o > \frac{\hbar q_y^2}{F_n^2 e}. \tag{3}$$

Diagrams for the zeroth-order terms of H' are shown in Fig. XI-1b. Here the

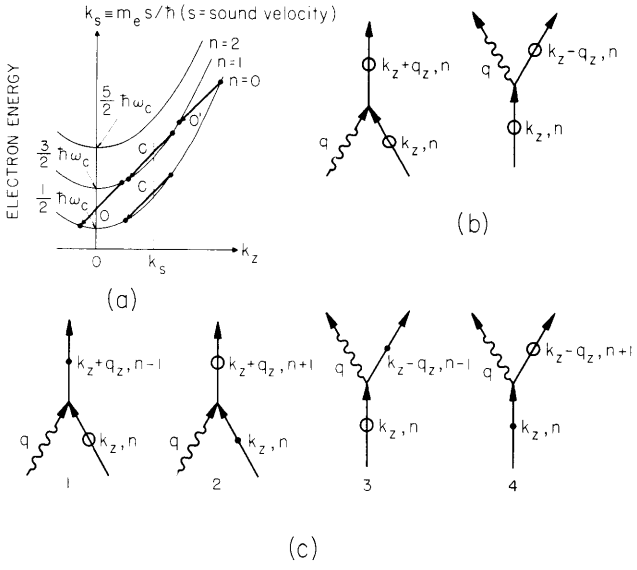

Fig. XI-1. (a) Landau-level diagram and examples of the two types of transitions.
(b) Diagrams for phonon emission and absorption resulting from the intra-Landau level.
(c) Diagrams for phonon emission and absorption resulting from the inter-Landau level transitions. Circles and dots indicate changes in the electron radius of gyration.

electron makes transitions within a Landau level without changing its radius of gyration. This is shown by arrows "C" in Fig. XI-1a and is essentially the same as the (stimulated) Cherenkov process. In this process the magnetic field does not play an important role, except for the effect of the overlap integral ξ_n, and in the classical limit $\hbar \to 0$ the interaction is independent of the magnetic field. The first-order terms in H' are shown in Fig. XI-1c, where circles and dots represent the change in radius of gyration. Diagram 3 in this figure shows emission of a phonon by electron transitions from a higher to a lower Landau level, which decreases its radius of gyration ("O" in Fig. XI-1a). Diagram 4 shows emission of a phonon by electron transitions from a lower to a higher Landau level, which increases its radius of gyration (O' in Fig. XI-1a). These processes are essentially the interaction between waves and moving oscillators.[6, 7] In the classical limit they correspond to the Doppler-shifted cyclotron resonance interaction.[8]

The time rate of generation of stimulated phonons $\left(n_q^{-1}\, dn_q/dt \equiv \gamma\right)$ is obtained from time-dependent perturbation theory. The results may be summarized as follows.

For intra-Landau level (Cherenkov) processes

$$\gamma_C = \frac{C^2 m^2 \omega_c q}{2\pi\rho\hbar^3 \omega_q |\cos\theta|} \sum_n \left[(f_n(K_+) - f(K_-)\right] \frac{2}{\pi} \int_0^{\pi/2} \left[\xi_n\{q \sin\theta \sin\phi\}\right]^2 d\phi, \tag{4}$$

where

$$K_\pm = (m/\hbar)(s/\cos\theta - v) \pm (1/2)\, q \cos\theta, \tag{5}$$

θ is the angle between the magnetic field B_o and the phonon wave vector, s is the sound velocity, and v is the electron drift velocity.

For inter-Landau level (oscillator-wave) processes

$$\gamma_{OW} = \left(\frac{C^2 m^2 \omega_c q}{2\pi\rho\hbar^3 \omega_q |\cos\theta|}\right)\left(\frac{\hbar q^2 \sin^2\theta}{2m\omega_c}\right)$$

$$\times \sum_n (n+1)\{f_n(K'_+) - f_{n+1}(K'_-) + f_{n+1}(K''_+) - f_n(K''_-)\}$$

$$\times \frac{2}{\pi} \int_0^{\pi/2} \cos^2\phi\, \xi_n(q \sin\theta \sin\phi)\, \xi_{n+1}(q \sin\theta \sin\phi)\, d\phi, \tag{6}$$

where

$$K'_\pm = K_\pm + m\omega_c/\hbar q \cos\theta \tag{7}$$

$$K''_\pm = K_\pm - m\omega_c/\hbar q \cos\theta \tag{8}$$

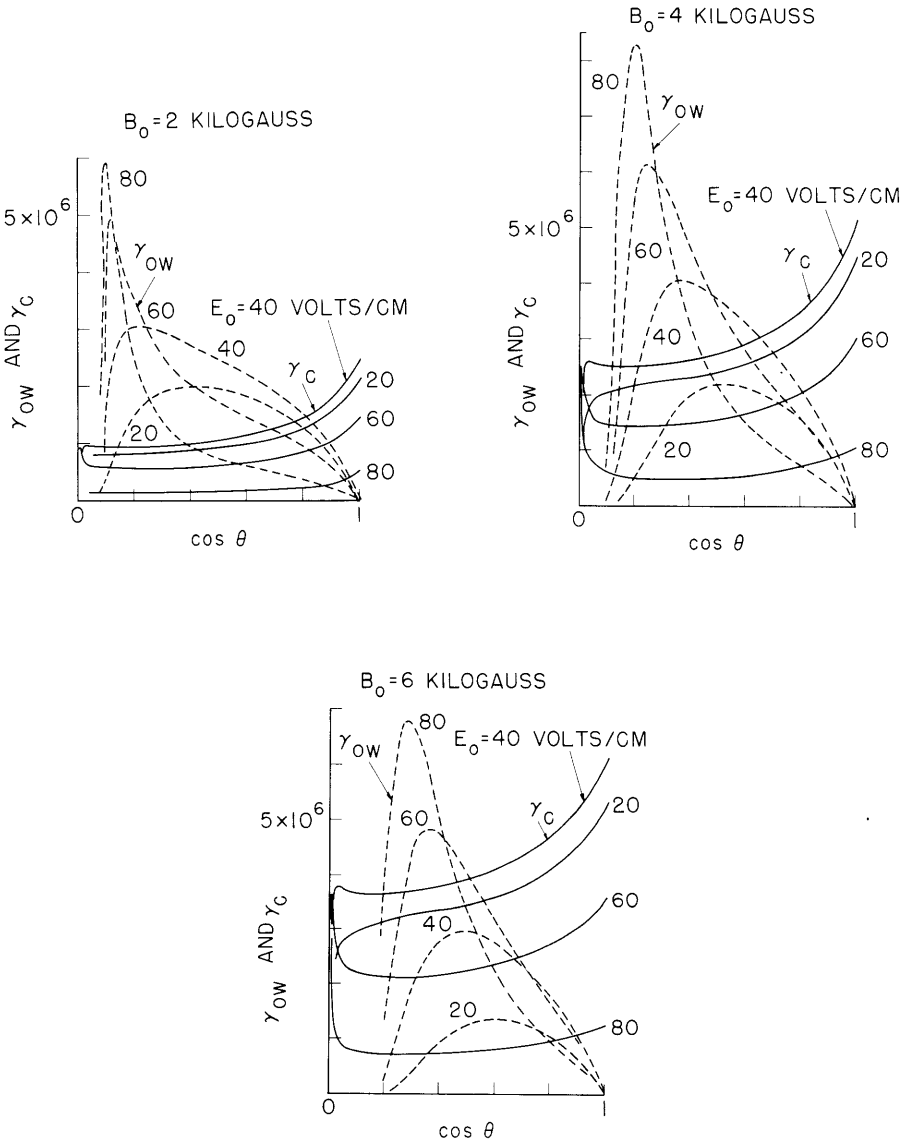

Fig. XI-2. Time rate (γ) of generation of stimulated phonons as a function of angle of emission (θ) with respect to the applied magnetic field, and for various values of B_o and E_o.

In (4) and (6) f is the Fermi distribution function,

$$f_n(K) = \{1 + \exp[\hbar^2K^2/2m+(n+1/2)\hbar\omega_c - \epsilon_F]/kT\}^{-1}. \quad (9)$$

Net stimulated emission of phonons ($\gamma > 0$) is obtained when the electrons have sufficient drift, and γ exceeds the decay rate of phonons because of other processes.

Our analysis was stimulated by recent experiments[1,2] that show microwave emission from an n-type InSb bar in parallel electric and magnetic fields. For our experiments[2] at 9.3 kmc we used n-type InSb at 77°K with electron concentration of 2×10^{14} cm^{-3}, mobility 10^6 cm^2/volt sec, and the results were $q \times$ (electron mean-free path) ≈ 15, $q \times$ (Debye length) ≈ 15, and at 5 kgauss $\omega_c\tau \approx 60$, $\hbar\omega_c \approx kT_e$ (T_e=100°K), and $q \times$ (electron gyration radius) < 1 for $n < 8$. Hence, by using C = 30 ev,[9] (4) and (6) can be used to evaluate γ as a function of θ. The results are shown in Fig. XI-2. We note that for certain angles θ the inter-Landau level process can dominate. The sharp decrease in γ for small cos θ is due to the integrals of $\xi_n\xi_{n+1}$ and is approximately predicted by (3). Figure XI-3 shows the maximum growth rate for the inter-Landau level process as a function of magnetic field B_o. The threshold magnetic field corresponds closely to the magnetic field at which we observe the onset of enhanced microwave emission. The threshold electric field, which is also observed experimentally, would be determined from the condition that γ exceed the phonon decay rate resulting from other processes. At present, there are no data available on the lifetime of 10-kmc phonons in InSb at 77°K. The coupling of the phonons to the microwave field in the waveguide must be assumed to occur at the boundary of the InSb bar.

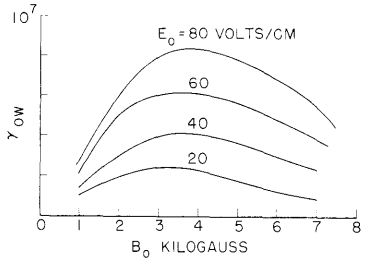

Fig. XI-3. Maximum (with respect to θ) time rate of generation of phonons as a function of the applied magnetic field, for various values of the applied electric field.

T. Musha, A. Bers

References

1. S. J. Buchsbaum, A. G. Chynoweth, and W. L. Feldmann, Appl. Phys. Letters 6, 67 (1965).

2. T. Musha and A. Bers, "Electron-Phonon Instabilities in a Magnetic Field," a paper presented at the Solid-State Device Research Conference, Princeton University, Princeton, New Jersey, June 21-23, 1965; the experiments reported in this paper are the same as those of Buchsbaum, Chynoweth, and Feldmann,[1] except at 10 kmc.

3. C. Kittell, Quantum Theory of Solids (John Wiley and Sons, Inc., New York and London, 1963), Chap. 11.

4. Ibid., pp. 23 and 132.

5. L. I. Schiff, Quantum Mechanics (McGraw-Hill Book Company, Inc., New York, Toronto, and London, 2d edition, 1955), Chap. 4.

6. V. L. Ginzburg, Soviet Phys. – Usp. 2, 874 (1960).

7. T. Musha, J. Appl. Phys. 35, 3273 (1964).

8. Doppler-shifted cyclotron resonance interaction between electrons and phonons for crossed electric and magnetic fields has been treated by H. N. Spector, Phys. Rev. 131, 2512 (1963).

9. E. Haga and H. Kimura, J. Phys. Soc. Japan 18, 777 (1963).

2. LONGITUDINAL INTERACTION OF ELECTRONS WITH PHONONS IN A MAGNETIC FIELD

In order to gain a more complete picture of electron-phonon interactions we shall attempt to formulate it in terms of a dispersion relation that contains the interactions self-consistently. In the future we shall analyze the nature of the stability of these interactions. First, we give our results of a classical self-consistent field analysis, and then the quantum-mechanical analysis. Both analyses will be for longitudinal acoustic and electron-plasma waves ($\bar{q} \parallel \bar{E}$), at an arbitrary angle to the applied magnetic field, and coupled through the deformation potential.

Classical Formulation

The equation of motion for the lattice displacement, $\bar{\xi}$, is

$$\rho \ddot{\bar{\xi}} = \nabla \cdot \bar{\bar{T}} + C\nabla n - m^* n(\dot{\bar{\xi}} - \bar{v})\,\nu, \tag{1}$$

where ρ is the mass density, $\bar{\bar{T}}$ is the stress tensor, C is the deformation potential coupling constant, n is the electron density, m^* is the electron effective mass, $\bar{v}$ is the electron velocity, and ν is the effective electron-lattice collision frequency. The electron distribution function f is taken to satisfy the Boltzmann equation and is assumed to relax to the local equilibrium function

$$\frac{\partial f}{\partial t} + \bar{w} \cdot \frac{\partial f}{\partial \bar{r}} - \frac{e}{m}\left(\bar{E} - \frac{m\nu}{e}\dot{\bar{\xi}} + \bar{w} \times \bar{B}_o\right) \cdot \frac{\partial f}{\partial \bar{w}} = -\nu\left(f - f_o - \frac{n}{n_o} f_o - \dot{\bar{\xi}} \cdot \frac{\partial f_o}{\partial \bar{w}}\right), \tag{2}$$

where f_o is the unperturbed electron distribution function, n_o is the unperturbed electron density, and $\bar{B}_o$ is the applied magnetic field.

We linearize Eqs. 1 and 2 and solve them together with Poisson's equation. Assuming a dependence $\exp(-i\omega t + i\bar{q} \cdot \bar{r})$, we find that the resultant dispersion relation is

$$K_p + K_e - 1 = 0, \tag{3}$$

where

$$K_p = \frac{\omega^2 - q^2 s^2 + i\omega\nu \dfrac{m^* n_o}{\rho}}{\omega^2 - q^2 s^2 + i\omega\nu \dfrac{m^* n_o}{\rho} + \dfrac{C^2 \epsilon_L}{\rho e^2} q^4 \left(1 - i\omega\nu \dfrac{m^*}{Cq^2}\right)^2} \tag{4}$$

$$K_e = 1 - \frac{\dfrac{\omega_p^2}{q^2} \displaystyle\int_{-\infty}^{\infty} dw_{||} \int_0^{\infty} dw_\perp \, w_\perp 2\pi \sum_n \frac{J_n^2(p)\left(\dfrac{n\omega_c}{w_\perp} \dfrac{\partial f_o}{\partial w_\perp} - q_{||} \dfrac{\partial f_o}{\partial w_{||}}\right)}{(\omega + i\nu - q_{||} w_{||} - n\omega_c)}}{1 + i\nu \displaystyle\int_{-\infty}^{\infty} dw_{||} \int_0^{\infty} dw_\perp \, w_\perp \, 2\pi f_o \sum_n \frac{J_n^2(p)}{(\omega + i\nu - q_{||} w_{||} - n\omega_c)}} . \tag{5}$$

Here, s is the sound velocity, ω_p is the electron plasma frequency, ω_c is the electron cyclotron frequency, $q_{||}$ is the wave number component along B_o, $q_\perp$ is the wave number component across B_o, and $p = q_\perp w_\perp / \omega_c$.

If the unperturbed electron distribution function is taken as a Maxwellian with thermal velocity $v_T = \kappa T/m$, and shifted along the magnetic field with drift velocity v_D, Eq. 5 may be written in terms of the plasma dispersion function $Z(\zeta)$,[1]

$$K_e = 1 + \frac{\dfrac{\omega_p^2}{q^2 v_T^2}\left[1 + \displaystyle\sum_n I_n(\lambda)\, e^{-\lambda}\, \zeta_o Z(\zeta_n)\right]}{1 + \dfrac{i\nu}{q_{||} v_T \sqrt{2}} \displaystyle\sum_n I_n(\lambda)\, e^{-\lambda}\, Z(\zeta_n)}, \tag{6}$$

where

$$\zeta_n = \frac{\omega + i\nu - q_{||} v_D - n\omega_c}{q_{||} v_T \sqrt{2}} \tag{7}$$

$$\lambda = \left(\frac{q_\perp v_T}{\omega_c}\right)^2 . \tag{8}$$

Computations on instabilities contained in Eqs. 3-8 are in progress.

Quantum-Mechanical Formulation

To account for quantum-mechanical effects in the interaction we formulate the electron part of the dispersion relation, K_e, in terms of the single-particle density matrix ρ,

including a phenomenological damping term. Previous formulations either do not account for collisions,[2] or include collisions but with relaxation to an equilibrium that has no density fluctuations.[3] For our interests in longitudinal oscillations we choose a collision description with relaxation to local equilibrium, that is, with a perturbed density.

$$\frac{\partial \rho}{\partial t} + \frac{i}{\hbar}[H, \rho] = -\frac{1}{\tau}\left\{\rho - \left(1 + \frac{n_1}{n_o} I\right) \rho_o\right\}, \tag{9}$$

where I is a matrix, each element of which is unity, H is the Hamiltonian, ρ_o is the density matrix for the steady state, n_1 and n_o are, respectively, fluctuating and averaged electron densities, and [,] is the commutation bracket. The relaxation terms on the right-hand side of (9) imply that ρ is relaxing with the time constant τ to the local equilibrium, which to first order is given by $(1+n_1 I/n_o)\rho_o$. For longitudinal waves with dependence $\exp(i\omega t - i\bar{q}\cdot\bar{r})$, we obtain

$$K_e = 1 - \frac{\dfrac{m\omega_p^2}{q^2 n_o} \displaystyle\sum_{\nu,\nu'} \frac{\rho_o(E_\nu) - \rho_o(E_{\nu'})}{E_\nu - E_{\nu'} - \hbar(\omega - i/\tau)} \xi^2_{\nu',\nu}}{1 - i\dfrac{\hbar}{\tau}\dfrac{1}{n_o} \displaystyle\sum_{\nu,\nu'} \frac{\rho_o(E_\nu)}{E_\nu - E_{\nu'} - \hbar(\omega - i/\tau)} \xi^2_{\nu',\nu}}, \tag{10}$$

where E_ν is the electron energy of the state ν specified by (k_y, k_z, n), and $\xi_{\nu',\nu}$ is the overlap integral as used in Sec. XI-A.1.

Assuming that the unperturbed electron velocity distribution is Maxwellian with thermal velocity v_T and drift velocity v_D, we obtain

$$K = 1 - \frac{\dfrac{m\omega_p^2}{q^2} \displaystyle\sum_{N,\mu} \frac{1 - e^{-\hbar\omega_c/mv_T^2}}{\sqrt{2}\,\hbar v_T q_{||}} \left\{ Z\left(\zeta_\mu + \frac{\hbar q_{||}}{2\sqrt{2}\,mv_T}\right) e^{-\mu\hbar\omega_c/mv_T^2} - Z\left(\zeta_\mu - \frac{\hbar q_{||}}{2\sqrt{2}\,mv_T}\right)\right\} \xi^2_{N+\mu,N}\, e^{-N\hbar\omega_c/mv_T^2}}{1 - i\dfrac{\hbar}{t} \displaystyle\sum_{N,\mu} \frac{1 - e^{-\hbar\omega_c/mv_T^2}}{\sqrt{2}\,\hbar v_T q_{||}} Z\left(\zeta_\mu + \frac{\hbar q_{||}}{2\sqrt{2}\,mv_T}\right) \xi^2_{N+\mu,N}\, e^{-N\hbar\omega_c/mv_T^2}} \tag{11}$$

Here, ξ is as defined in Eq. 7. In the classical limit $\hbar \to 0$, the quantum-mechanical formulation (11) agrees exactly with the classical formulation (6). Computations on electron-phonon interactions using Eqs. 3, 4, and 11 are also in progress.

A. Bers, T. Musha

References

1. B. D. Fried and S. D. Conte, The Plasma Dispersion Function (Academic Press, Inc., New York, 1961).

2. J. J. Quinn and S. Rodriguez, "Electrodynamic Properties of a Quantum Plasma in a Uniform Magnetic Field," Phys. Rev. 128, 2487 (1962).

3. S. Tosima, J. J. Quinn, and M. A. Lampert, "Effect of Collisions on the Magneto-conductivity Tensor of a Quantum Plasma," Phys. Rev. 137, A883 (1965).

B. INSTABILITIES OF WAVES ACROSS THE MAGNETIC FIELD

1. INSTABILITIES IN TRANSVERSE WAVES ALONG B_0

In previous reports we have discussed instabilities in transelectromagnetic waves that propagate along an applied magnetic field in a plasma with anisotropic velocity distribution of electrons.[1, 2] In this report we consider the extent of the damping of the instabilities arising from finite electron temperature along the magnetic field. We also show that the plasma dispersion equation contains a negative energy wave associated with the zero-order transverse energy. The instabilities are interpreted in terms of the coupling between this wave and the well-known passive right circularly polarized waves in the plasma. Further details may be found in Robertson's thesis.[3]

Damping of the Instabilities

For an electron velocity distribution of the form

$$f_0(v_\perp, v_\parallel) = \frac{1}{2\pi v_\perp}\,\delta(v_\perp - v_{0\perp})\,\delta(v_\parallel - v_{0\parallel}) \tag{1}$$

a simultaneous solution of the relativistic Vlasov equation and Maxwell's equation yields the dispersion relation[2]

$$\frac{C^2k^2}{\omega^2} = 1 - \frac{\omega_p^2(\omega - kv_{0\parallel})}{\omega^2(\omega - kv_{0\parallel} - \omega_b)} - \frac{\omega_p^2 v_{0\perp}^2(k^2 - \omega^2/c^2)}{2(\omega - kv_{0\parallel} - \omega_b)^2} \tag{2}$$

for right circularly polarized waves with dependence $e^{j(\omega t - kz)}$. Following the Bers-Briggs criterion for instability, we plot the real k locus in the complex ω-plane. The

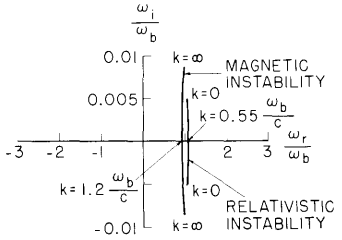

Fig. XI-4. Real k locus for $v_{0\parallel} = 0$.

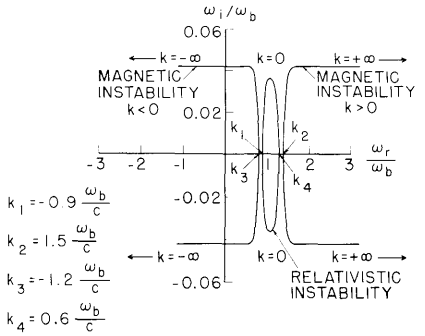

Fig. XI-5. Real k locus for finite $v_{0\parallel}$.

locus for $v_{0\|} = 0$ is given in Fig. XI-4, and for finite $v_{0\|}$ in Fig. XI-5. Two unstable branches are distinguished. A "magnetic instability," caused by first-order forces on the electron exerted by the first-order magnetic field of the wave, is found for wave numbers with magnitude greater than ω_b/c. A "relativistic instability," caused by the relativistic change in the cyclotron frequency of the electrons as they interact with the wave is found at wave numbers with magnitude less than ω_b/c.

For an electron distribution of the form

$$f_0(v_\perp, v_\|) = \frac{1}{(2\pi)^{3/2} v_{T\|} v_\perp} \delta(v_\perp - v_{0\perp}) \exp\left[-\frac{(v_\| - v_{0\|})^2}{2v_{T\|}^2}\right], \tag{3}$$

where $v_{T\|}$ is the electron temperature along B_0, the dispersion relation is

$$\frac{C^2k^2}{\omega^2} = 1 - \frac{\omega_p^2}{\omega^2}\left[1 - \frac{\omega_b}{\sqrt{2}\, kv_{T\|}} H(\zeta)\right] + \frac{\omega_p^2}{\omega^2} \frac{v_{0\perp}^2}{2v_{T\|}^2 k^2}\left(k^2 - \frac{\omega^2}{c^2}\right)(1+\zeta H(f)), \tag{4}$$

where

$$H(\zeta) = \frac{1}{\sqrt{\pi}} \int_{-\infty}^{\infty} \frac{e^{-x^2}}{x - \zeta} dx; \qquad I_m \zeta < 0 \tag{5}$$

and

$$\xi = \frac{\omega - kv_{0\|} - \omega_b}{\sqrt{2}\, kv_{T\|}}. \tag{6}$$

The real k locus obtained from (4) is given in Fig. XI-6 for $v_{0\|} = 0$, and in Fig. XI-7 for finite $v_{0\|}$. (The scale in Fig. XI-6 is expanded to show the details.) As is evident from the figures, the magnetic instabilities for large wave numbers are damped by the longitudinal temperature. As the temperature is increased, the damping of the magnetic instabilities extends to lower and lower wave numbers. From Fig. XI-7 it is evident that there are 6 wave numbers at which the plasma experiences a transition from stable to unstable. These wave numbers are defined as k_1-k_6 in Fig. XI-8. The relativistic instability exists for wave numbers between k_3 and k_4. The negative wave number branch of the magnetic instability exists between wave numbers k_1 and k_2, and the positive wave number branch between k_5 and k_6.

There is a physical reason why the magnetic instability is not found at wave numbers less than ω_b/c. The magnetic instability requires that there be some electrons in resonance with the wave. No electrons can have velocities along the magnetic field greater than c. Thus the upper limit on the phase velocity of an unstable wave is c. Since the

instability occurs near $\omega \cong \omega_b$, the lower limit on the wave number of the magnetic instability is near ω_b/c. Note that the relativistic instability that does not arise from such a wave resonance condition can have waves with phase velocities greater than c.

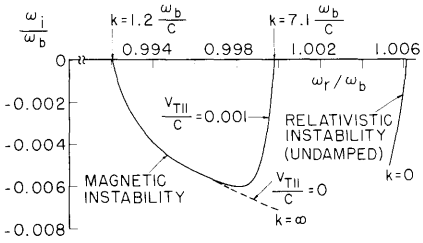

Fig. XI-6.
Zero drift real k locus for finite temperature.

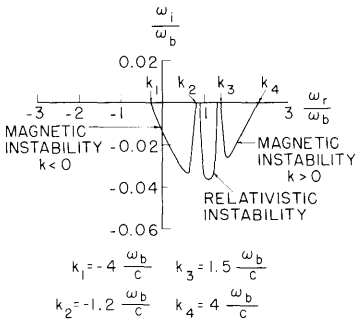

Fig. XI-7.
Finite drift real k locus with finite temperature.

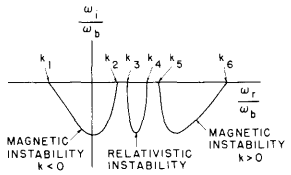

Fig. XI-8.
Characteristic shape of real k locus defining transition wave.

The temperature at which the magnetic instability disappears is found by obtaining the temperature at which $k_1 = k_2$ or $k_6 = k_5$. The transition wave numbers k_2 and k_5 can be found from the zero temperature dispersion relation (Eq. 2). The plasma becomes unstable near $\omega \approx \omega_d + kv_{0\parallel} = \omega_d$. Setting $\omega = \omega_d$ and solving the quadratic in Eq. 2 for $\omega - \omega_d$ yields

$$\omega - \omega_d = -\frac{\omega_p^2\omega_b}{2\left(c^2k^2-\omega_d^2\right)} \pm \left\{\left[\frac{\omega_p^2\omega_b}{2\left(c^2k^2-\omega_d^2\right)}\right]^2 - \frac{\omega_p^2 v_{0\perp}^2}{2c^2}\right\}^{1/2} . \tag{7}$$

The instabilities set in when the radical in Eq. 7 is zero. Setting the radical to zero yields for the transition wave numbers

$$\frac{k_2 c}{\omega_b} = \frac{\frac{v_{0\parallel}}{c} - \left[1 + \frac{\omega_p c}{\sqrt{2}\,\omega_b v_{0\perp}}\left(1 - \frac{v_{0\parallel}^2}{c^2}\right)\right]^{1/2}}{1 - \frac{v_{0\parallel}^2}{c^2}} \tag{8}$$

and

$$\frac{k_5 c}{\omega_b} = \frac{\frac{v_{0\parallel}}{c} + \left[1 + \frac{\omega_p c}{\sqrt{2}\,\omega_b v_{0\perp}}\left(1 - \frac{v_{0\parallel}^2}{c^2}\right)\right]^{1/2}}{1 - \frac{v_{0\parallel}^2}{c^2}}. \tag{9}$$

The transition wave numbers k_1 and k_6 are found by a method that is due to Sudan.[4] The dispersion relation is written as

$$k^2 = \frac{\pi\omega_p^2}{c^2 - \frac{\omega^2}{k^2}} \int_0^\infty dv_\perp \int_{-\infty}^\infty dv_\parallel \left[\frac{v_\perp^2 \left(v_\parallel - \frac{\omega}{k}\right) \frac{\partial f_o}{\partial v_\perp}}{v_\parallel - \left(\frac{\omega}{k} - \frac{\omega_b}{k}\right)} - \frac{v_\perp^3 \frac{\partial f_o}{\partial v_\parallel}}{v_\parallel - \left(\frac{\omega}{k} - \frac{\omega_b}{k}\right)} \right] = R\left(\frac{\omega}{k}\right). \tag{10}$$

At the transition wave numbers ω and k are pure real. The Cauchy type of integral in Eq. 10, split into its real and imaginary parts, yields the equation for the transition wave numbers k_1 and k_6:

$$k^2 c^2 \left(1 - \frac{v_{0\parallel}^2}{c^2}\right) + 2kv_{0\parallel}\omega_b \left(\frac{2v_{T\parallel}^2}{v_{0\perp}^2} - 1\right) - \omega_b^2 \left(\frac{2v_{T\parallel}^2}{v_{0\perp}^2} - 1\right)^2 - \omega_p^2 \frac{\left(1 - \frac{2v_{T\parallel}^2}{v_{0\perp}^2}\right)}{\frac{2v_{T\parallel}^2}{v_{0\perp}^2}} = 0. \tag{11}$$

The solutions from (11) are set equal to the solutions from (8) and (9), thereby resulting in the solution for the thermal velocity at which the magnetic instability disappears. The

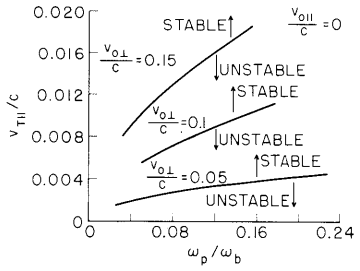

Fig. XI-9. Temperature at which magnetic instability disappears.

numerical solution for $v_{T\parallel}/c$ is shown in Fig. XI-9 as a function of ω_p/ω_b for several values of $v_{0\perp}/c$, for the case $v_{0\parallel} = 0$. From Fig. XI-9 it is evident that $\left(2v_{T\parallel}^2/v_{0\perp}^2\right) \ll 1$, for which an approximate solution for the thermal velocity at which the magnetic instability is damped as

$$\frac{v_{T\parallel}}{c} \approx \left[\frac{\omega_p v_{0\perp}^3}{\sqrt{2}\,\omega_b c^3}\right]^{1/2} . \tag{12}$$

The relativistic instability was found undamped for the nonrelativistic temperatures considered.

Mode-Coupling Picture of the Instabilities

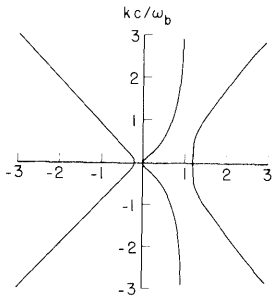

Fig. XI-10. Dispersion diagram for a cold plasma.

In Fig. XI-10 the k - vs - ω dispersion diagram is plotted for a cold plasma (Eq. 2 with $v_{0\perp}=0$). In Fig. XI-11 the dispersion diagram is plotted for finite $v_{0\perp}$. Conditions have been chosen in Fig. XI-11 such that the relativistic instability does not exist. The region of the magnetic instability where ω is complex for real k is shown as a dashed line. From Fig. XI-11 it is evident that the plasma with finite transverse energy contains a new wave branch. This wave branch satisfies the approximate relation

$$\omega \cong \omega_b + kv_{0\parallel} \tag{13}$$

The small-signal, time-averaged energy in the plasma can be calculated[5, 6] from

$$\langle w_r \rangle = \tfrac{1}{4}\mu_0 |H|^2 + \tfrac{1}{4}\epsilon_0 |E|^2 \frac{\partial(\omega K_r)}{\partial\omega}, \tag{14}$$

where K_r is the right-hand element of the dielectric tensor in rotating coordinates. From the dispersion relation the small-signal energy is calculated to be

$$\frac{\langle w_r \rangle}{\frac{1}{4}\epsilon_0 |E|^2} = 2 + \frac{\omega_p^2 \omega_b}{\omega(\omega - kv_{0\parallel} - \omega_b)} - \frac{\omega_p^2 v_{0\perp}^2}{\omega c^2} \frac{[\omega(\omega_b + kv_{0\parallel}) - c^2k^2]}{(\omega - kv_{0\parallel} - \omega_b)^3}. \tag{15}$$

For the cold ($v_{0\perp}=0$) plasma of Fig. XI-10 all waves have positive energy and the plasma supports only passive waves. For the plasma with transverse energy ($v_{0\perp}\neq 0$) of Fig. XI-11 the new wave branch represented by Eq. 13 has been found to carry negative energy. The small-signal energy of this wave branch is plotted as a function of wave

number in Fig. XI-12.

The large wave number instability (magnetic instability) can be seen (Fig. XI-11) to

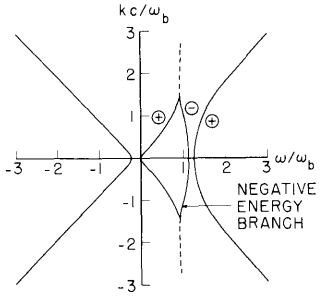

Fig. XI-11. Dispersion diagram for a plasma with zero-order energy transverse to B_0; ⊕ indicates a positive energy branch; ⊖ indicates a negative energy branch.

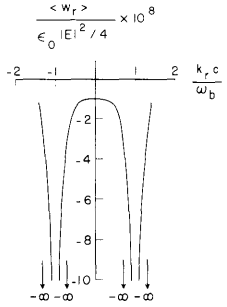

Fig. XI-12. Small signal energy of active wave branch.

arise from coupling of the negative energy branch with the right circularly polarized branch below ω_b. Since both branches have $k \to \infty$ for $\omega \to \omega_b$, this instability exists for any finite $v_{0\perp}$. The relativistic instability, which occurs for small wave numbers, arises because of coupling between the negative energy branch and the right circularly polarized branch above ω_b. For the parameters of Fig. XI-11 there is no such coupling. But, if either (ω_p/ω_b) is decreased (which moves the passive branch to lower frequencies) or $(v_{0\perp}/c)$ is increased (which moves the active branch to higher frequencies), the coupling will set in. As can be seen from Fig. XI-11, the waves that then couple have opposite group velocities, and we would expect absolute (nonconvective) instabilities to arise. We have determined that the absolute instabilities, which we have previously found from our exact computations,[1, 2] are indeed predicted by the coupling described here. Furthermore, the coupling picture clearly shows how the relativistic instability may disappear with increasing (ω_p/ω_b).

E. A. Robertson, A. Bers

References

1. A. Bers, J. K. Hoag, and E. A. Robertson, "Instabilities in Transverse Waves along B_0 for Beam-type Distributions," Quarterly Progress Report No. 77, Research Laboratory of Electronics, M.I.T., April 15, 1965, pp. 149-152.

2. E. A. Robertson and A. Bers, "Instabilities of Transverse Waves along the Magnetic Field," Quarterly Progress Report No. 78, Research Laboratory of Electronics, M.I.T., July 15, 1965, pp. 105-110.

3. E. A. Robertson, "Plasma Instabilities in Transverse Waves along the Magnetic Field," S.M. Thesis, Department of Electrical Engineering, M.I.T., Cambridge, Mass., August 24, 1965.

4. R. N. Sudan, "Plasma Electromagnetic Instabilities," Phys. Fluids 6, 57 (1963).

5. A. Bers, "Properties of Waves in Time- and Space-Dispersive Media," Quarterly Progress Report No. 65, Research Laboratory of Electronics, M.I.T., April 15, 1962, pp. 89-93.

6. A. Bers, "Energy and Power in Media with Temporal and Spacial Dispersion," Quarterly Progress Report No. 66, Research Laboratory of Electronics, M.I.T., July 15, 1962, pp. 111-116.

2. INSTABILITIES IN QUASI-STATIC WAVES ACROSS B_0

We have continued[1] the study of instabilities of quasi-static waves ($\bar{k}$ parallel to $\bar{E}$) propagating perpendicular to a static uniform magnetic field in an infinite plasma composed of stationary ions and electrons with an unperturbed distribution function

$$f_0 = \frac{1}{2\pi p_{\perp 0}} \delta(p_\perp - p_{\perp 0})\, \delta(p_{||}) \tag{1}$$

Here, $p_\perp$ is the magnitude of the momentum across the magnetic field, and $p_{||}$ is the momentum along the field. The dispersion relation for quasi-static waves propagating across the field has been shown[1, 2] to be

$$K_L(\omega, k_\perp) = 1 - \frac{\omega_p^2}{k^2} \sum_{n=-\infty}^{\infty} \left\{ \frac{k^2 \left(J_{m-1}^2 - J_{m+1}^2\right)}{2\omega_b(\omega - m\omega_b)} - \frac{m^2 \omega_b^2 J_m^2}{c^2(\omega - m\omega_b)^2} \right\} = 0. \tag{2}$$

This was obtained from a dielectric tensor description of the plasma that is consistent with the complete set of Maxwell's equations and the relativistic Vlasov equation.[3] Here, ω_p and ω_b are the (relativistic) electron plasma and cyclotron frequencies, respectively, c is the velocity of light, and J_m is the n^{th}-order Bessel function of the first kind and argument $(k_\perp p_{\perp 0}/M\omega_b)$.

The dispersion relation has been solved numerically for the roots $\omega = \omega(k_\perp)$. In our work an instability is said to exist when ω has a negative imaginary part for a real $k_\perp$. The criteria for classifying the type of instability (convective or absolute) has not been applied. Two distinct types of instabilities have been found.

The first type of instability had been predicted previously by a nonrelativistic analysis performed by Harris, Dory, and Guest,[4] although they did not determine the form of the dispersion characteristics. Their dispersion relation is obtained from (2) by

letting $c \to \infty$ and interpreting ω_p and ω_b as the nonrelativistic quantities. The "zero-frequency" instability that we reported also is an example of this kind of instability.[1] The study has now been extended to higher frequencies. Figure XI-13 is the dispersion diagram obtained from the nonrelativistic equation for a plasma whose density is such that $\omega_p/\omega_b = 1.5$. Note that there is a single passband at the cyclotron frequency and at each of its harmonics. The dispersion characteristics display an oscillatory behavior about the harmonic frequency. All passbands but the fundamental begin at $\omega = m\omega_b$. The fundamental begins at the hybrid frequency, $\omega = \left(\omega_b^2 + \omega_p^2\right)^{1/2}$. Figure XI-14 shows a higher density plasma with $\omega_p = 2.1\ \omega_b$. This plasma is similar to the one just discussed in that the waves are still purely propagating. But the branch of the dispersion characteristics which may be associated with the cyclotron fundamental at large values of $k_\perp$ now starts at $\omega = 2\omega_b$. It is the first harmonic that begins at the hybrid frequency. Note also that the amplitude of the oscillation of the root locus about each harmonic has increased. Figure XI-15 illustrates the dispersion characteristics of a still higher density plasma. With $\omega_p = 2.75\ \omega_b$, bands of unstable wavelengths are observed. By comparing Figs. XI-14 and XI-15 it can be seen that the amplitude of the oscillations of the root locus has become great enough for neighboring modes to overlap. This appears to happen for all modes studied at a density such that $\omega_p = 2.5\ \omega_b$. Figure XI-16, which has been drawn for a still higher density plasma, $\omega_p = 4.25\ \omega_b$, shows that increasing the density also increases the widths of the unstable bands. Also, we observe the onset of the "zero-frequency" instability. Figure XI-17 illustrates the growth rates (ω_c/ω_b) for the two unstable cases discussed above. The magnitude of the growth rate is seen to increase with increasing density. These two cases indicate, however, that it is not always the fundamental that has the maximum growth. Although more data should be taken to confirm this view, we feel that for a fixed plasma density the growth maximizes at a particular harmonic.

The small-signal time-averaged energy density for quasi-static waves in a dispersive medium[5] is given by

$$\langle \omega \rangle = \frac{1}{4}\epsilon_0 |E|^2 \left[\omega \frac{\partial K_L}{\partial \omega}\right]_{K_L=0}. \tag{3}$$

In Figs. XI-18 and XI-19 we plot the energy density of the fundamental and first harmonic when $\omega_p = 2.1\ \omega_b$. Note that at the points where the two modes are closest in Fig. XI-14, one wave (the harmonic) carries negative small-signal energy, while the other carries positive. This behavior is observed in all of the modes. When the frequency is above the harmonic the small-signal energy is positive, and it is negative when below. Thus, the high-density instabilities may be interpreted in terms of an internal coupling of an active wave (negative small-signal energy) with a passive one. The "zero-frequency"

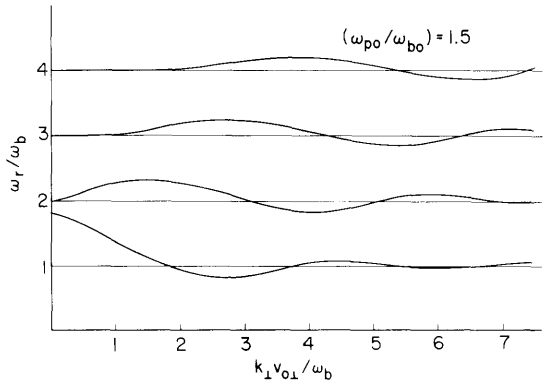

Fig. XI-13.

Nonrelativistic dispersion diagram for $(\omega_{p0}/\omega_{b0}) = 1.5$.

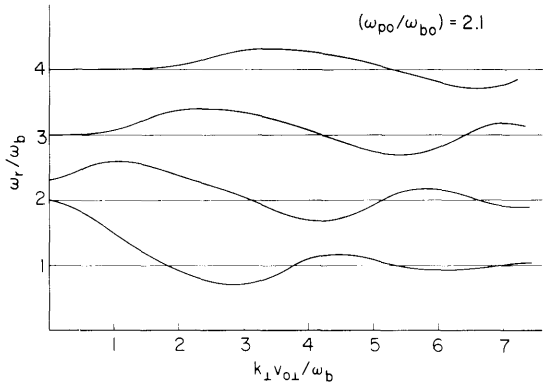

Fig. XI-14.

Nonrelativistic dispersion diagram for $(\omega_{p0}/\omega_{b0}) = 2.1$.

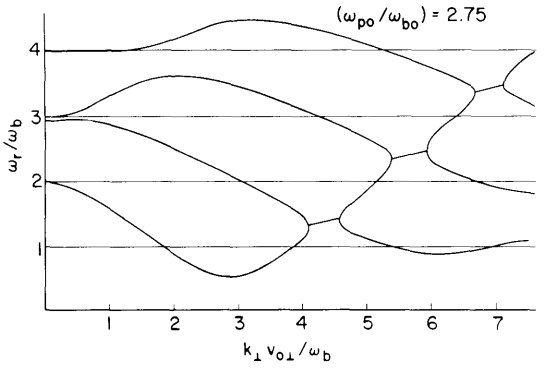

Fig. XI-15.

Nonrelativistic dispersion diagram for $(\omega_{p0}/\omega_{b0}) = 2.75$.

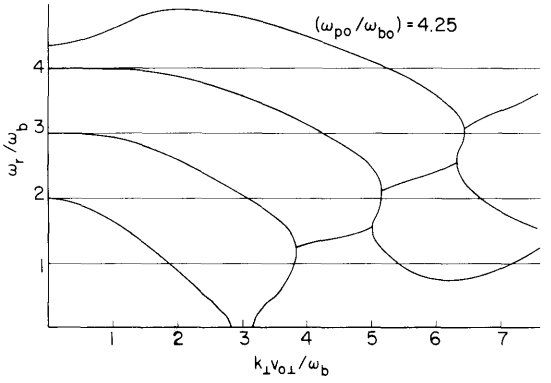

Fig. XI-16.

Nonrelativistic dispersion diagram for $(\omega_{p0}/\omega_{b0}) = 4.25$.

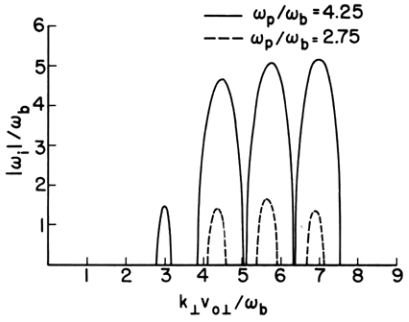

Fig. XI-17.

Growth rates for the high density instability.

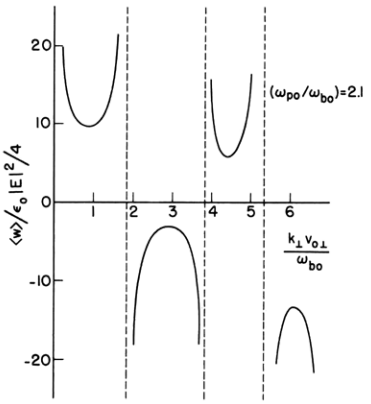

Fig. XI-18.

Small-signal energy of the fundamental. $(\omega_{p0}/\omega_{b0}) = 2.1$.

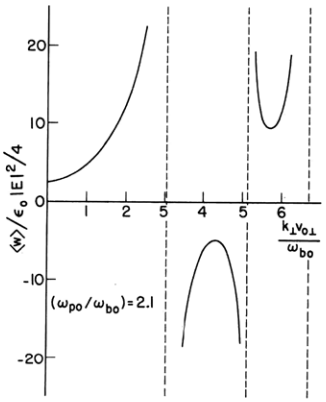

Fig. XI-19.

Small-signal energy of the first harmonic. $(\omega_{p0}/\omega_{b0}) = 2.1$.

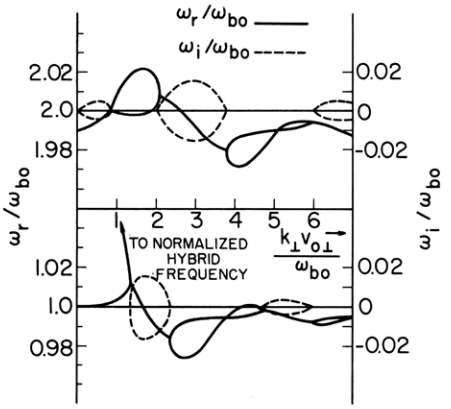

Fig. XI-20.

Relativistic dispersion of the fundamental and first harmonic. $(\omega_{p0}/\omega_{b0}) = 0.5$.

instability is interpreted as a coupling of the mode starting at $\omega = 2\omega_b$ (see Figs. XI-15 and XI-16) with the one that would start at $\omega = -2\omega_b$. (The dispersion relation is symmetrical in ω.) A numerical calculation has shown, however, that both waves carry negative small-signal energy.

The second type of instability observed in this plasma appears only in a relativistic analysis. The relativistic dispersion relation predicts two roots near each harmonic, while the nonrelativistic equation predicts only one. Figure XI-20 shows the root locus of the fundamental and first harmonic of a plasma in which $\omega_p = 0.5\ \omega_b$. The nonrelativistic analysis predicted no unstable waves at this low density; however, here we see bands of unstable wavelengths. Expanding Eq. 2 near the m^{th} harmonic and keeping terms only to second order in $(p_{\perp 0}/Mc)$, we find that the plasma is unstable at the m^{th} harmonic if

$$\frac{\omega_p/\omega_b}{p_{\perp 0}/Mc} < \frac{1}{|J'_m|}, \tag{4}$$

where the prime indicates the derivative with respect to the argument of the Bessel function. Since J'_m vanishes at discrete values of its argument $(k_\perp p_{\perp 0}/M\omega_b)$, the plasma is always unstable in bands of wavelengths about these points. The widths of these bands are always nonzero for finite (ω_p/ω_b). It is possible that this relativistic instability is more important than the high-density instabilities discussed earlier because they appear at such low densities. Note, however, that the new roots of the relativistic equation lie extremely close to the cyclotron harmonic frequencies. The validity of the quasi-static approximation used in obtaining Eq. 2 from the dielectric tensor may be in question for these roots. Further study requires that this approximation be checked. We are at present doing this.

C. E. Speck, A. Bers

References

1. C. Speck and A. Bers, Quarterly Progress Report No. 78, Research Laboratory of Electronics, M.I.T., July 15, 1965, pp. 110-114.
2. C. E. Speck, "Quasi-Static Theory of Plasma Instabilities at Cyclotron Harmonics," S.M. Thesis, Department of Electrical Engineering, M.I.T., Cambridge, Mass., September 1965.
3. A. Bers, "Dispersion Relations for Plasmas in a Magnetic Field, III," Internal Memorandum, Research Laboratory of Electronics, M.I.T., Cambridge, Mass., August 1964.
4. E. G. Harris, R. A. Dory, and G. E. Guest, "Unstable Plasma Waves Propagating Perpendicular to a Magnetic Field," Phys. Rev. Letters 5, 131-133 (1965).
5. A. Bers and S. Gruber, "Negative-Energy Plasma Waves and Instabilities at Cyclotron Harmonics," Appl. Phys. Letters 6, 27-28 (1965).
6. A. Bers, "Instabilities in Plasmas with Beam-type Distributions" (Abstract to appear in Bull. Am. Phys. Soc.)

C. QUASI-LINEAR INTERACTION OF A FILAMENTARY ELECTRON BEAM WITH A PLASMA-FILLED WAVEGUIDE

1. Introduction

In the last few years, a number of authors have examined the nonlinear aspects of the beam-plasma interaction using the methods of quasi-linear theory.[1-3] Several have considered the development of instabilities in an infinite plasma resulting from a "single-shot" injection of a beam. That is, the initial distribution function is taken as that of a plasma and a monoenergetic beam, and this distribution function is allowed to relax in time because of the development of the instability. This situation is shown in Fig. XI-21a. Because of spatial symmetry, these nonlinear solutions are independent of all spatial coordinates. While these studies provide some insight into the behavior of beam-plasma systems, they have little relevance to those beam-plasma experiments in which the beam is continuously injected into the plasma region.

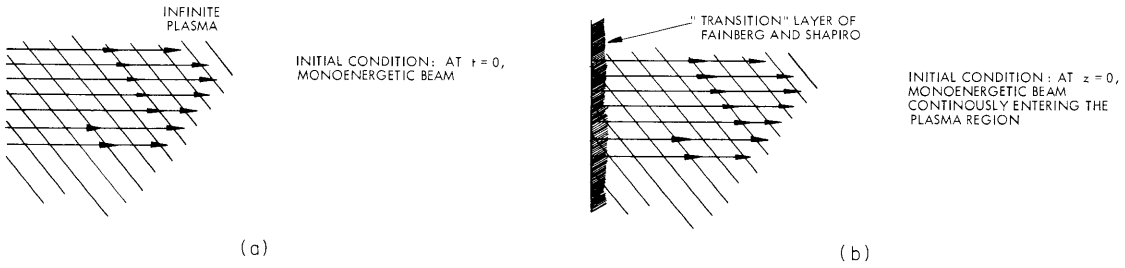

Fig. XI-21. (a) Single-shot injection of a beam into an infinite plasma.
(b) Continuous injection of a beam into a semi-infinite plasma.

Recently, Fainberg and Shapiro[3] have studied a semi-infinite plasma into which a monoenergetic electron beam is continuously injected. This is illustrated in Fig. XI-21b. They find that a "transition" layer is formed at the plasma boundary, z = 0, because of the instabilities that develop. This layer is a region of large and highly inhomogeneous electric field strength. Most of the beam energy is lost in passing through this layer, and the beam itself emerges from the layer highly diffused in velocity space. These authors find that the thickness of this layer tends to zero on a time scale of a few tenths of a microsecond for typical beam and plasma parameters. To keep the layer thickness finite, one must postulate a loss mechanism to remove energy from the boundary layer. Fainberg and Shapiro assume that the energy is transported away at the group velocity of the propagating plasma wave.

In this report we have analyzed a problem in which a monoenergetic electron beam of finite transverse dimensions in continuously injected into a circular plasma waveguide.

The beam velocity v_o at the entrance plane z = 0 is taken to be much greater than the plasma thermal velocity, v_T. The ratio of beam to plasma radius, b/a, is taken to be «1, and the plasma frequency ω_p, beam plasma frequency ω_{pb}, and electron cyclotron frequency ω_{ce} are assumed to satisfy the condition $\omega_{ce} \ll \omega_{pb} \ll \omega_p$. Only circularly symmetric solutions of the nonlinear equations will be considered. Under these assumptions, the beam-plasma system supports only a convective instability, and the electric field strength according to linear theory increases exponentially away from the beam entrance plane. Figure XI-22 shows the geometry of the system that we analyze.

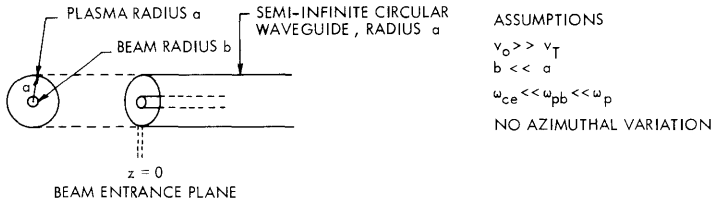

Fig. XI-22. Geometry of the beam-plasma system.

Since the beam density n_b is much less than the plasma density n_p, the important nonlinear effects occur in the beam alone. Therefore we treat the plasma as linear and solve for the beam distribution function in the steady-state limit $t \to \infty$. From this function we obtain the average beam velocity $\overline{v_o(z)}$ and the beam temperature $T_b(z)$ in the steady state.

2. Linear Theory of the Interaction between a Filamentary Electron Beam and a Plasma Waveguide

The dispersion equation of the beam-plasma system shown in Fig. XI-22 is

$$\beta(\omega) = \frac{\omega}{v_o} \frac{1}{1 \mp j\sqrt{-\dfrac{F(q)\,\omega_{pb}^2 b^2}{2v_o^2 K_\perp(\omega)}}} \tag{1}$$

where

$$F(q) = \ln \frac{1}{qb} + \frac{\pi}{2} \frac{N_o(qa)}{J_o(qa)} \tag{2}$$

and p and q are the transverse wave numbers in the beam and plasma regions, respectively. The transverse dielectric constant $K_\perp$ is given by

$$K_\perp = \frac{\omega^2 - \omega_+^2}{\omega^2 - \omega_{ce}^2}, \tag{3}$$

where

$$\omega_+^2 = \omega_p^2 + \omega_{ce}^2. \tag{4}$$

Figure XI-23 is a sketch of the dispersion function (1). It is seen from (1) that complex roots of β for real ω are obtained when $K_\perp$ is negative. The complex root with

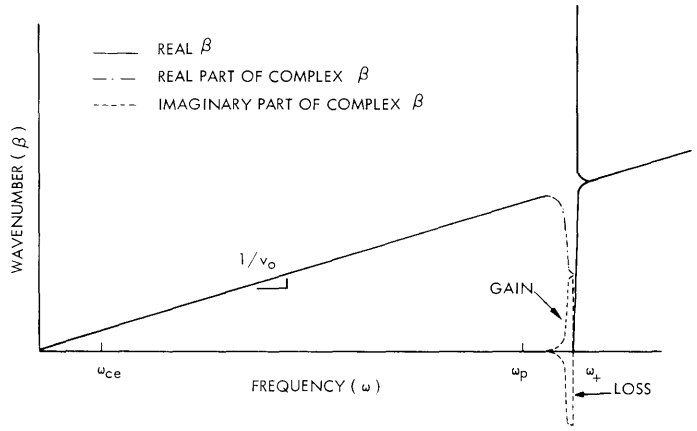

Fig. XI-23. Reactive-medium dispersion function for the n = 0 mode.

$\beta_i > 0$ is an amplifying wave, since for $\omega_i \to -\infty$ both roots of β from (1) are in the lower half β-plane. The amplification rate β_i is given by

$$\beta_i = \frac{\omega}{v_o} \frac{Q(\omega)}{1 + Q^2(\omega)}, \tag{5}$$

where

$$Q(\omega) = \sqrt{-\frac{F(q)\,\omega_{pb}^2 b^2}{2v_o^2 K_\perp(\omega)}} \tag{6}$$

provided Q is real. The condition of maximum gain is given by $Q^2 = 1$, for which the maximum gain is

$$\beta_{iMAX} = \frac{\omega_{MAX}}{2v_o} \tag{7}$$

and the frequency of maximum gain is

$$\omega_{MAX} = \omega_+ \sqrt{1 - \frac{1}{2}\frac{\omega_{pb}^2}{v_o^2} F(q)\, b^2} \tag{8}$$

The "half-power" width of the gain curve is

$$\Delta\omega = \sqrt{2}\,\omega_+ F(q) \frac{\omega_{pb}^2}{v_o^2} b^2 \tag{9}$$

in the limit $\frac{\omega_{pb}}{v_o} b \ll 1$. We shall use (7) and (9) below where a nonlinear equation describing the filamentary beam-plasma waveguide system is formulated.

It can be shown that for the system of Fig. XI-23 the filamentary beam approximation is valid, provided that $b\omega_p/2v_o \lesssim 0.1$. Furthermore, although this system supports an absolute instability at beam synchronism with the propagating plasma wave, it can be shown that the growth rate in time, ω_i, of this absolute instability is very small compared with the frequency of the oscillations, ω_p. The addition of even a small amount of collisional damping in the plasma would serve to supress the absolute instability, since the growth rate, ω_i, is so very small. Such damping would reduce the large reactive medium amplification rate (7) but slightly. Accordingly, we assume that the absolute instability is suppressed, and ignore it in the rest of this report.

3. Quasilinear Theory of the Filamentary Beam Distribution Function

We shall study the distribution function of the electron beam using the methods of quasi-linear theory. The beam distribution function $f(\bar{r}, \bar{v}, t)$ is described by the nonlinear Vlasov equation:

$$\frac{\partial f}{\partial t} + \bar{v} \cdot \frac{\partial f}{\partial \bar{r}} + \frac{q}{m}(\bar{E} + \bar{v} \times \bar{B}_o) \cdot \frac{\partial f}{\partial \bar{v}} = 0, \tag{10}$$

where $\bar{B}_o = \bar{i}_z B_o$ is the static magnetic field. The nonlinearity arises because $\bar{E}$ is itself a function of f.

$$\frac{\partial}{\partial \bar{r}} \cdot \bar{E}(\bar{r}, t) = \frac{q}{\epsilon_o}\left[n_b \int f\, d\bar{v} + n_p \int f_p\, d\bar{v} - n_b - n_p\right]. \tag{11}$$

Usually, (10) is linearized about a known "operating point" or steady-state distribution $f_o(\bar{v})$ by assuming that

$$f(\bar{r}, \bar{v}, t) = f_o(\bar{v}) + f_1(\bar{r}, \bar{v}, t). \tag{12}$$

In quasi-linear theory, the linearized solutions are used to evaluate the nonlinear term of (10) and the Vlasov equation is resolved. Provided the linear solution f_1 is much smaller than the exact (and unknown) nonlinear solution f, the separation of f into a zero and first-order distribution function is still useful. The zero-order distribution function f_o must now be considered to vary with r and t. Thus we write for the system of Fig. XI-23:

$$f(\bar{r}, \bar{v}, t) = f_o(\bar{r}, \bar{v}, t) + f_1(\bar{r}, \bar{v}, t), \tag{13}$$

where

$$f_1(\bar{r}, \bar{v}, t) = \sum_{n=1}^{2} \int_{-\infty}^{\infty} d\omega\, f_{n\omega}(\bar{v})\, J_o(p_n(\omega) r)\, \exp[j(\omega t - \beta_n(\omega) z)] \tag{14}$$

In (14), the summation over n represents a sum over the plus and minus signs of the reactive medium dispersion equation (1). Both roots must be included in f_1. The ω integration extends over negative, as well as positive, frequencies. The quantity $f_{n\omega}(\bar{v})$ represents the "Fourier coefficient" of the linearized solution at the real frequency ω. The wave numbers $p_n(\omega)$ and $\beta_n(\omega)$ are in general complex. It should be apparent that the significant contribution to the ω integral comes from the small ω regions where the reactive medium gain in high.

We also write

$$\bar{E}(\bar{r}, t) = \bar{E}_1(\bar{r}, t) = -\frac{\partial \Phi_1(\bar{r}, t)}{\partial \bar{r}}, \tag{15}$$

where

$$\Phi_1(\bar{r}, t) = \sum_{n=1}^{2} \int_{-\infty}^{\infty} d\omega\, \Phi_\omega J_o(p_n(\omega) r)\, \exp[j(\omega t - \beta_n(\omega))]. \tag{16}$$

Now Φ_ω and $f_{n\omega}(\bar{v})$ are related by the linearized Vlasov equation. In the filamentary beam limit, we obtain

$$f_{n\omega}(\bar{v}) = -\frac{q}{m} \frac{\beta_n(\omega) \frac{\partial f_o}{\partial v_z}}{\omega - \beta_n(\omega) v_z} \Phi_\omega. \tag{17}$$

The nonlinear equation describing the rate of change of the zero-order beam distribution function $f_o(\bar{r}, \bar{v}, t)$ will now be derived. We first insert the linear solutions (14-16) into the nonlinear Vlasov equation (10). Now in the linear theory, f_o is independent of time. Accordingly, in the quasi-linear theory, we assume $f_o(\bar{r}, \bar{v}, t)$ to be a weakly

varying function of time, and we average Eq. 10 over a time, T, satisfying the following inequality

$$\frac{2\pi}{\omega_{MAX}} \ll T \ll \frac{2\pi}{\Delta\omega}, \tag{18}$$

where ω_{MAX} and $\Delta\omega$ are given by (8) and (9), respectively. The time-average equation becomes

$$\frac{\partial f_o}{\partial t} + \bar{v} \cdot \frac{\partial f_o}{\partial \bar{r}} + \frac{q}{m} \bar{v} \times \bar{B}_o \cdot \frac{\partial f_o}{\partial \bar{v}} + 2 \frac{q}{m} \Delta\omega \sum_{n=1}^{2} \sum_{n'=1}^{2} \int d\omega \, \Phi_\omega \left[\left(-\frac{\partial}{\partial \bar{r}} \right) J_o(p_n(\omega) r) \, e^{-j\beta_n(\omega) z} \right]$$

$$\cdot \frac{\partial f_{n'\omega}(\bar{v})}{\partial \bar{v}} J_o(p_{n'}(-\omega) r) \, e^{-j\beta_{n'}(-\omega) z} = 0 \tag{19}$$

Taking the filamentary beam limit, performing the summations and integration, and using (17), (7), (8), and (9), we find

$$\frac{\partial f_o}{\partial t} + v_z \frac{\partial f_o}{\partial z} + 2(\Delta\omega)^2 |\Phi_\omega|^2 \frac{q^2 \omega_+}{m^2 v_o} e^{\frac{\omega_+}{v_o} z} \frac{\partial}{\partial v_z} \frac{\partial f_o}{\partial v_z} \frac{v_z}{-v_z^2 - 2v_o^2 + 2v_o v_z} = 0. \tag{20}$$

This is the equation we sought. It is a real, linear equation describing the change in the zero-order beam distribution function $f_o(\bar{r}, \bar{v}, t)$. We now solve (20) in the steady state $\frac{\partial f_o}{\partial t} = 0$. The equation is then separable. We normalize (21) by the substitutions

$$\epsilon_o = \frac{q^2}{m^2} \frac{2(\Delta\omega)^2}{v_o^4} |\Phi_\omega|^2$$

$$z' = \frac{\omega_+}{v_o} z$$

$$v' = \frac{v_z}{v_o}.$$

Then (20) becomes

$$\frac{\partial f_o}{\partial z'} e^{-z'} + \epsilon_o \frac{1}{v'} \frac{\partial}{\partial v'} \left(\frac{\partial f_o}{\partial v'} \frac{v'}{-v'^2 + 2v' - 2} \right) = 0. \tag{21}$$

Assuming a separation $f_o(z', v') = g(z') h(v')$, we obtain

$$g(z') = \exp[K(1 - e^{z'})] \tag{22}$$

and

$$\frac{d}{dv'}\left(\frac{dh(v')}{dv'}\,\frac{v'}{-v'^2+2v'-2}\right)-Kv'h(v')=0, \tag{23}$$

where K is the separation constant. Let $v' = u + 1$ and assume that h(u) is small unless $u \approx 0$. Since at the beam entrance plane $h(u) = \delta(u)$, a delta function in velocity space, this limit should prove interesting. Letting $u \to 0$ in (23) yields

$$\frac{d^2h}{du^2}+\frac{dh}{du}+\frac{K}{\epsilon_o}h=0. \tag{24}$$

Equation 24 has exponential solutions $e^{j\gamma u}$, where $K = \epsilon_o(\gamma^2-j\gamma)$. Superposing these solutions with (22) and matching the boundary condition $f_o(u, z'=0) = \delta(u)$, we find

$$f_o(u,z')=\frac{1}{\sqrt{2\pi}\,v_T(z')}\exp\left[-\frac{(u+v_d(z))^2}{2V_T^2(z)}\right], \tag{25}$$

where

$$v_T^2(z')=2\epsilon_o(e^{z'}-1) \tag{26}$$

$$v_d(z')=\epsilon_o(e^{z'}-1). \tag{27}$$

The energy density U(z') of the beam is

$$U(z')=1+\epsilon_o^2(e^{z'}-1)^2, \tag{28}$$

and the beam electron density n_b is constant. The solution is plotted in Fig. XI-24a.

Summarizing these results, we have found that

1. The zero-order beam density n_b does not vary along the length of the beam.

2. The average velocity of the beam $\overline{v_o(z')} = v_o - v_d(z')$ decreases with increasing z according to (27). At first, $\overline{v_o(z')}$ decreases linearly with z', but after a distance ≈ 1, the decrease is exponential with z'. This decrease represents a loss of DC beam energy.

3. The beam acquires a longitudinal temperature, $\frac{kT_b(z')}{m} = v_T^2$, given by Eq. 26. The thermal velocity $v_T(z')$ increases initially as the square root of z'.

4. The DC energy density of the beam <u>increases</u> as z' is increased. This surprising result indicates that the beam extracts energy from the plasma.

5. The solution (25) does not obey the conservation laws. For example, electrons are not concerned, since

$$\frac{d}{dz}(n_o v_o(z)) \neq 0.$$

These results were obtained by approximating the velocity equation (23) by a second-order linear equation with constant coefficients (24). We might expect that if (23) were solved exactly, these results would be modified. In particular, the solution of (20) should obey the conservation laws, and the DC energy density of the beam should probably decrease with increasing z'.

Since the analytical solutions (25) do not satisfy the conservation laws and lead to an increasing DC beam energy density, the exact solution of the diffusion equation (20) is of some interest. This equation has therefore been numerically integrated for $\epsilon_o = 0.01$ and z' in the range $0.4 < z' < 2.8$. The preliminary results of this numerical integration are presented in Fig. XI-24b. This figure should be carefully examined.

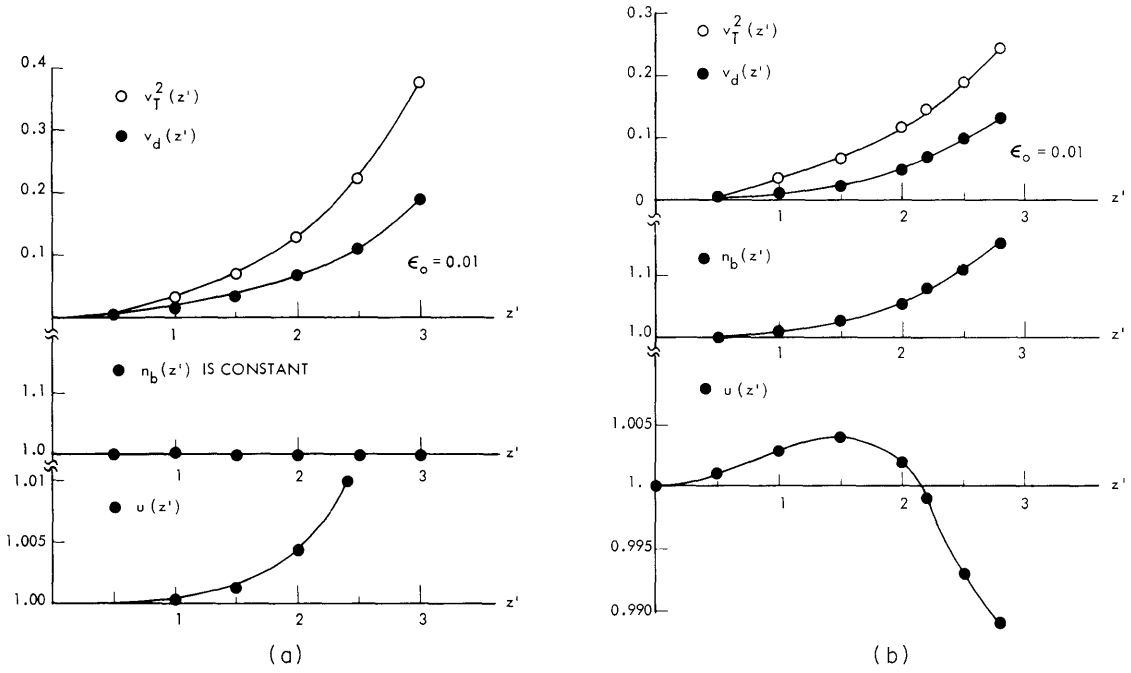

Fig. XI-24. Normalized thermal velocity v_T, velocity decrease of the beam v_d, beam density n_b, and beam energy density u as functions of z' (a) in the limit $f_o(v_z) \to 0$ unless $v_z \approx v_o$ and (b) computed exactly by numerical integration of Eq. 21.

First, note that the exact solution of (20) conserves electrons. The product $n_b(z')\overline{v_o(z')}$ is constant within one part in 10^4 over the range of z'. The beam density n_b is now an increasing function of z'. The velocities v_T and v_d are roughly similar to the approximate solutions in Fig. XI-24a; however, the DC energy density of the beam at first increases as in Fig. XI-24a, but then decreases as z' is increased. For

$z' > 2.1$, the average beam electron has lost energy. This energy must have been absorbed by the plasma; that is, the plasma has been heated by the beam.

M. A. Lieberman

References

1. Ya. A. Romanov and G. F. Filippov, Soviet Phys. – JETP 13, 87 (1961).
2. V. D. Shapiro, Soviet Phys. – JETP 17, 416 (1963).
3. Ya. B. Fainberg and V. D. Shapiro, Soviet Phys. – JETP 20, 4 (1965).

D. DISPERSION DIAGRAMS FOR HOT-ELECTRON PLASMAS

Computer solutions have been obtained for several beam-plasma dispersion equations. The computer program was described in Quarterly Progress Report No. 77 (pages 141-144). This program finds the zeros of a transcendental dispersion function $\underline{D}(\underline{\omega}, \underline{k}, \ldots)$ in the complex $\underline{\omega}$ or $\underline{k}$ plane.

1. Longitudinal Waves in an Infinite Maxwellian Plasma

Consider an electron beam of density n_b and velocity v_o immersed in an infinite, hot-electron plasma. The beam flows in the positive z direction, and all particle motion is assumed to be along z. The plasma electrons have a Maxwellian velocity distribution with thermal velocity v_T, while the plasma ions are assumed to be infinitely heavy. The dispersion equation for longitudinal (z-directed) waves in this system is

$$1 - \frac{\omega_{pb}^2}{(\omega - kv_o)^2} + \frac{1}{k^2\lambda_D^2}\left[1 + \frac{1}{\sqrt{2}\,k\lambda_D}\,\frac{\omega}{\omega_{pe}}\,Z\left(\frac{1}{\sqrt{2}\,k\lambda_D}\,\frac{\omega}{\omega_{pe}}\right)\right] = 0, \tag{1}$$

Where ω_{pb} and ω_{pe} are the beam and plasma frequencies, $\lambda_D = v_T/\omega_{pe}$ is the Debye wavelength, and $Z(\xi)$ is the plasma dispersion function tabulated by Fried and Conte.[1]

Three solutions of this dispersion equation are shown in Fig. XI-25. The dispersion equation (1) is solved under the assumption that the frequency $\underline{\omega}$ is pure real. Complex values of the wave number $\underline{k} = k_r + jk_i$ are thus obtained. The quantity k_i is the growth rate of the convective instability which this beam-plasma system supports. It is plotted as a dotted line in Fig. XI-25. The real wave number k_r is plotted as a solid line.

When the plasma thermal velocity v_T is zero, the dispersion equation can be solved exactly to yield

$$\underline{k} = \frac{\omega}{v_o} - \frac{\omega_{pb}}{v_o}\,\frac{\omega}{\sqrt{\omega^2 - \omega_{pe}^2}}. \tag{2}$$

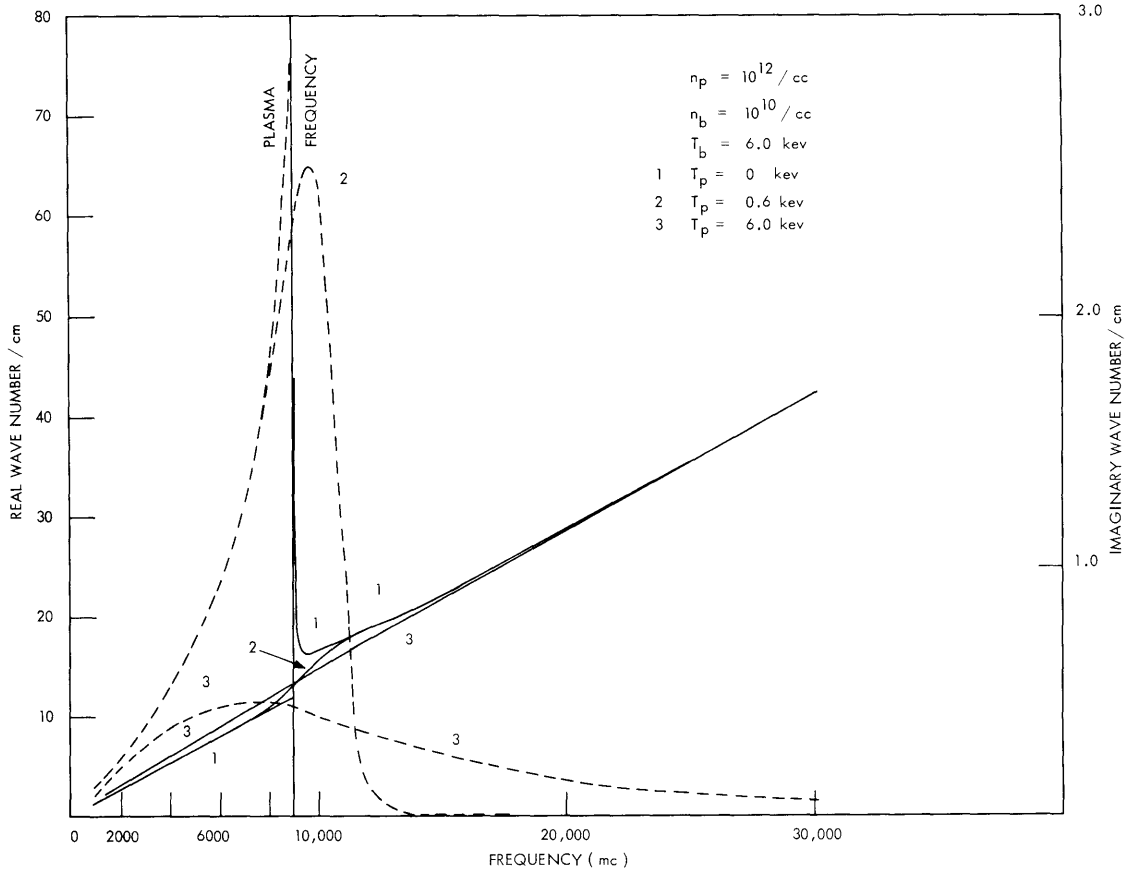

Fig. XI-25. Beam-plasma dispersion equation for longitudinal waves – Landau damping.

This well-known solution has an infinite growth rate k_i near $\omega = \omega_{pe}$. It is labeled (1) in Fig. XI-25.

The dotted curves labeled (2) and (3) in Fig. XI-25 are the corresponding growth rates when the electron thermal velocity v_T is finite. As v_T is increased, the gain k_i peaks at a finite value that decreases as v_T is increased. The frequency of maximum gain at first increases as v_T is initially increased from zero (curve (2)), but then decreases to fall below ω_{pe} for $v_T \gtrsim v_o$ (curve (3)). At the same time, the gain curve broadens as v_T is increased from zero. Physically, this broadening represents a kind of resistive medium amplification, in which the original "inductive" character of the plasma is diluted by a resistive component caused by the Landau damping in the plasma. As the thermal velocity v_T is increased above v_o, the peak gain $k_{i_{max}}$ must decrease, since the Landau damping of those plasma waves whose phase velocities coincide with v_o continually decreases.

2. Longitudinal Waves in a Cold-Ion, Hot-Electron Plasma

Consider now the dispersion equation

$$1 - \frac{\omega_{pi}^2}{\omega^2} - \frac{\omega_{pb}^2}{(\omega-\beta v_o)^2} + \frac{1}{k^2\lambda_D^2}\left[1 + \frac{1}{\sqrt{2}\,k\lambda_D}\frac{\omega}{\omega_{pe}} Z\left(\frac{1}{\sqrt{2}\,k\lambda_D}\frac{\omega}{\omega_{pe}}\right)\right] = 0 \tag{3}$$

in which the ions are now allowed to participate in the motion of the plasma. In the limit that the electron thermal velocity v_T is zero, this dispersion equation reduces to

$$1 - \frac{\omega_+^2}{\omega^2} - \frac{\omega_{pb}^2}{(\omega-\beta v_o)^2} = 0 \tag{4}$$

in which $\omega_+^2 = \omega_{pe}^2 + \omega_{pi}^2$, and ω_{pi} is the ion plasma frequency. Equation 4 has as its solution (2), in which ω_{pe}^2 is everywhere replaced by ω_+^2. Therefore, in the limit $v_T \to 0$, the gain is infinite for frequencies ω just below ω_+.

Consider now the limit $v_T \to \infty$. In this limit the dispersion equation (3) reduces to

$$1 - \frac{\omega_{pi}^2}{\omega^2} - \frac{\omega_{pb}^2}{(\omega-\beta v_o)^2} = 0 \tag{5}$$

which again has as its solution (2), in which ω_{pe}^2 is everywhere replaced by ω_{pi}^2. Therefore in the limit $v_T \to \infty$, the gain is infinite for frequencies ω just below ω_{pi}.

It is apparent from these considerations that a transition from a strong electron interaction to a strong ion interaction must occur as v_T is increased from zero. Briggs[2] considers this transition in a hot-electron plasma in which the electrons have a rectangular velocity distribution. He finds that an abrupt transition occurs when the parameter

$$\eta = \frac{n_b}{n_p}\frac{v_T^2}{2v_o^2} \tag{6}$$

is unity. For $\eta > 1$, a strong ion interaction occurs in which the gain is infinite for frequencies just below ω_{pi}. For $\eta < 1$, the ion interaction disappears, although the gain near the ion plasma frequency may still be finite.

In the weak beam limit $n_b \ll n_p$, the condition $\eta = 1$ requires $v_T \gg v_o$. Landau damping is small in this limit, so Briggs' results should hold for a Maxwellian hot-electron plasma. Figure XI-26 shows the exact solution of (3) in the weak beam limit. In Fig. XI-26a, $\eta = 1/2$ and no evidence of a strong ion interaction is apparent. Figure XI-26a is very similar to curve (3) of Fig. XI-25; that is, the gain mechanism in both curves is a resistive medium amplification.

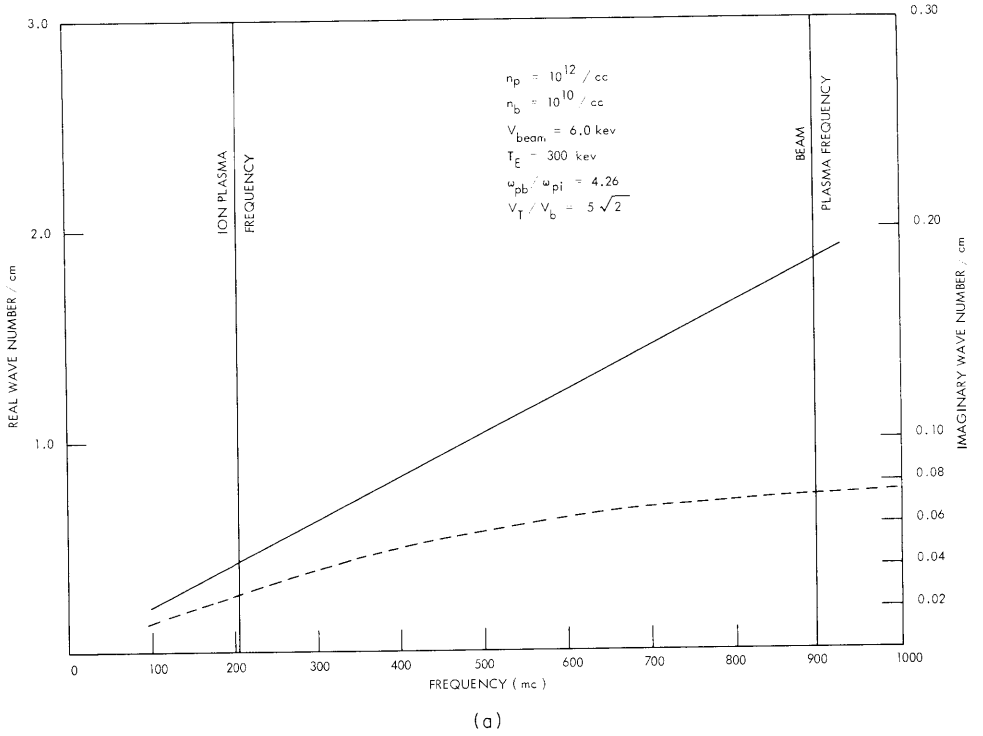

(a)

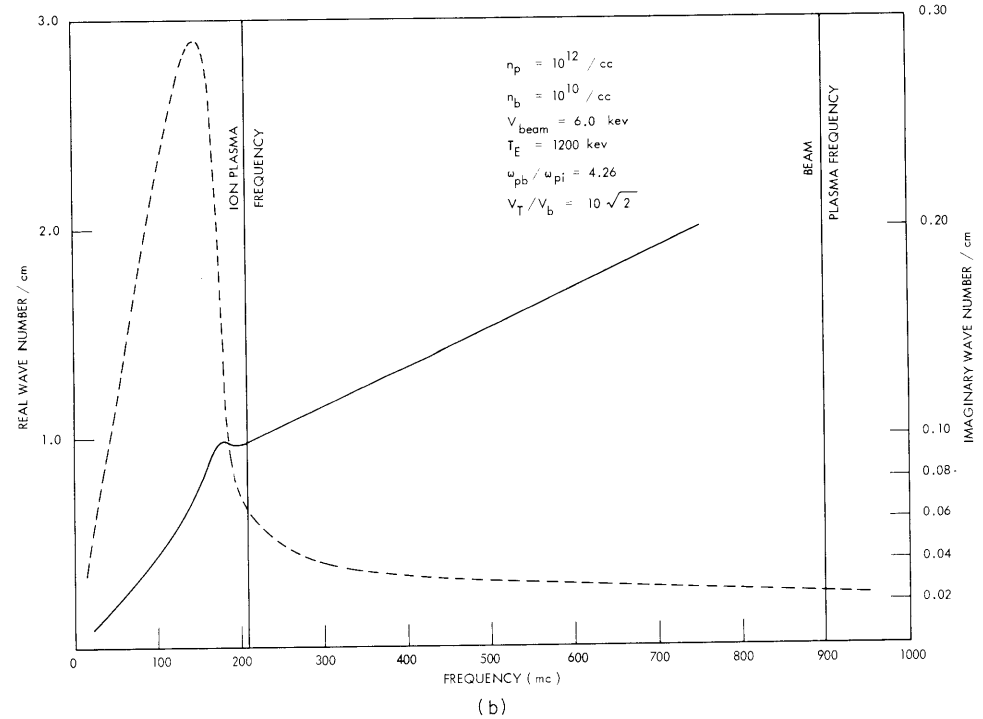

(b)

Fig. XV-26. Beam-plasma dispersion equation for longitudinal waves — Landau damping and ion motions included. (a) $\eta = 1/2$. (b) $\eta = 2$.

Figure XI-26b shows the case $\eta = 2$, for which Briggs' condition predicts a strong ion interaction. Such an interaction is indeed observed, although the gain is not infinite near the ion plasma frequency. The gain mechanism is clearly an interaction of the beam with the inductive plasma ions, degraded by the slight amount of Landau damping still present in the plasma. As η is further increased, the maximum gain near the ion plasma frequency must rapidly increase and tend to infinity as $\eta \to \infty$.

M. A. Lieberman

References

1. B. Fried and S. Conte, The Plasma Dispersion Function (Academic Press, New York, 1961).

2. R. J. Briggs, Electron-Stream Interaction with Plasmas (The M.I.T. Press, Cambridge, Mass., 1964).

E. NONADIABATIC DIFFUSION IN TOROIDAL GEOMETRY*

Construction of the toroidal device discussed in Quarterly Progress Reports No. 77 (pages 164-167) and No. 78 (pages 126-127) is nearly complete and tests are under way

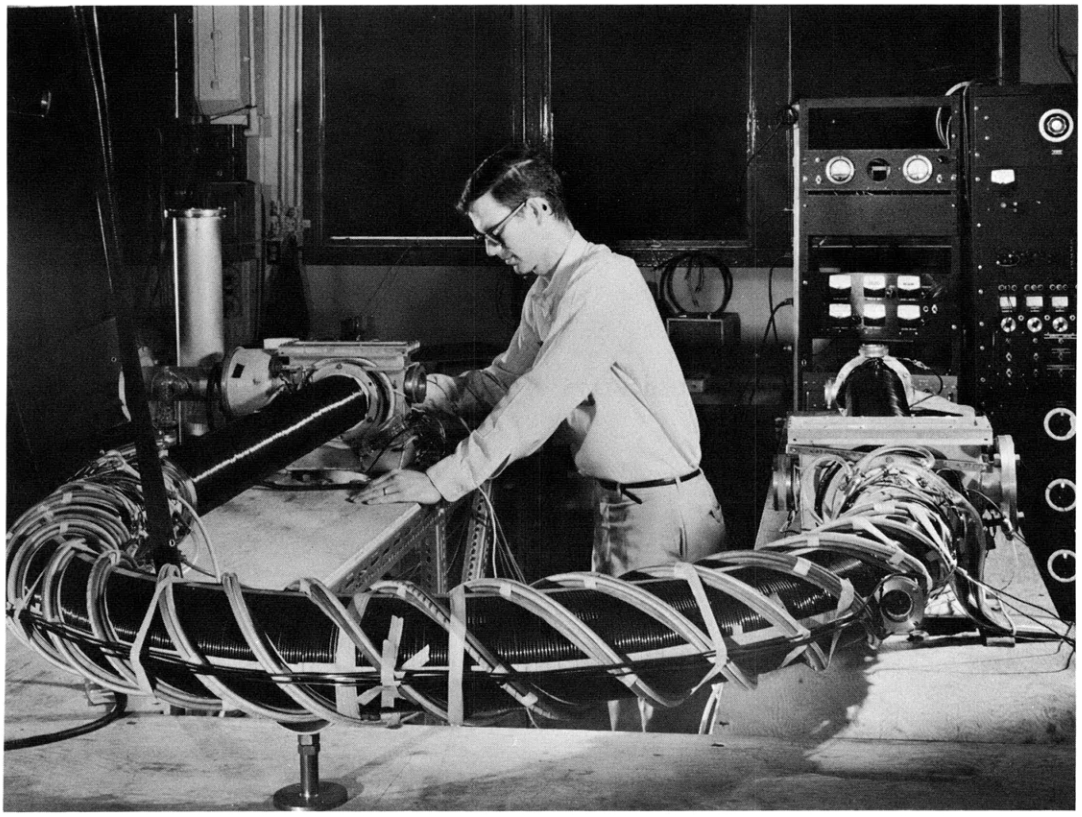

Fig. XI-27. Device for trapping an electron beam.

to determine the performance of one section of the device.

Figure XI-27 shows the device with one U bend removed for performance tests of the other U bend. These tests are performed by injecting an electron beam parallel to the field in the first straight section and observing visually the beam location at the entrance to the U bend by means of a fluorescent coated wire mesh that intercepts approximately 25 per cent of the beam. The beam is detected at the other end of the U bend by a fluorescent coated glass screen.

*This work was supported principally by the U.S. Atomic Energy Commission under Contract AT(30-1)-3285.

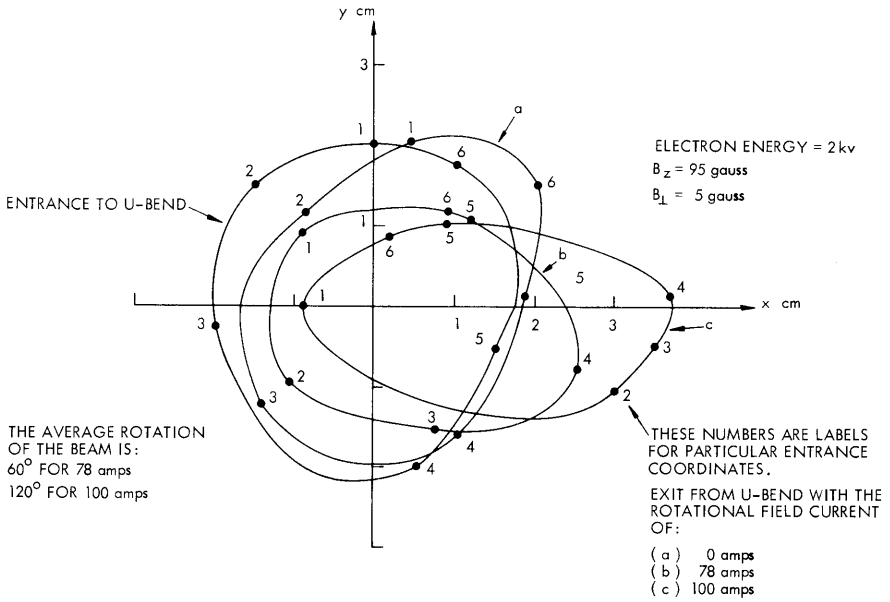

Fig. XI-28. Measured location of the input and output of the beam.

Figure XI-28 shows the location of the input and exit beams for various values of the rotational field. A vertical field, $B_\perp$, was produced on the U bend to just cancel the centripetal drift.

R. W. Moir, L. M. Lidsky

F. MEASUREMENT OF OPTICAL GAIN OF THE HOLLOW-CATHODE DISCHARGE*

Attempts by Edmonds, Gerry, and Lidsky[1] to observe laser action in a suitably configured argon hollow-cathode discharge (HCD) met with no success.

An experiment is in progress to measure directly the optical gain of the argon HCD at various wavelengths, including 4880Å and 5150Å. Our method is to direct a modulated light beam of the wavelength to be measured so that it passes axially through the HCD. The HCD is also modulated, but at a different frequency. Optical gain or absorption is manifested by an alternating component in the emergent light beam at frequencies equal to the sum and difference of the modulation frequencies of the HCD and incident light.

Preliminary results at 4880Å and 5150Å, obtained with the HCD of Edmonds, Gerry, and Lidsky, show no gain in excess of 0.1 per cent. The method indicates absorptions of 7 per cent 4804Å and 3 per cent at 4734Å.

M. D. Lubin

References

1. P. H. Edmonds, E. T. Gerry, and L. M. Lidsky, "The Hollow-Cathode Discharge as a Laser," Quarterly Progress Report No. 76, Research Laboratory of Electronics, M.I.T., January 15, 1965, pp. 129-130.

*This work was supported principally by the U.S. Atomic Energy Commission under Contract AT(30-1)-3285.

G. INTERACTION OF PARTICLES WITH CIRCULARLY POLARIZED WAVES IN PLASMAS*

The waves under discussion in this report are the right- and left-hand polarized waves moving with phase velocities very much less than that of light that appear in regions 8, 10, and 12 of the Allis diagram.[1] These are the regions in which one would expect the maximum wave activity in galactic plasmas on the basis of present density and magnetic field data. For such waves the ordinary linear dispersion relation can be written[2]

$$D_{LR} = k^2c^2 - \omega^2 - \frac{\omega_p^2\omega\pi}{n_s}\int_{-\infty}^{\infty} dv_{||}\int_0^{\infty} v_\perp^2\, dv_\perp \frac{\left\{\frac{\partial F}{\partial v} - \frac{v_{||}}{v_p}\frac{\partial F}{\partial v_\perp} + \frac{v_\perp}{v}\frac{\partial F}{\partial v_{||}}\right\}}{(\omega-\omega_o-kv_{||})} = 0, \qquad (1)$$

where v_p is the wave phase velocity, and ω_o is the gyro frequency.

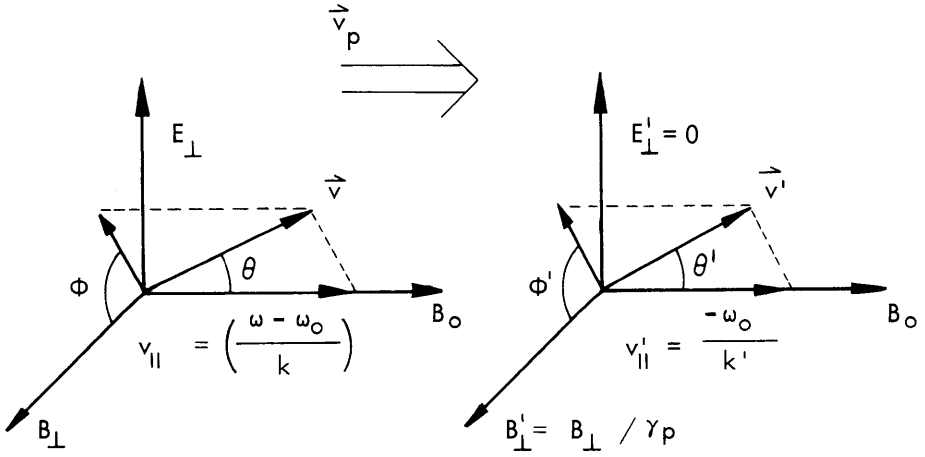

Fig. XI-29. Phase frame transform.

It is apparent that the growth or damping of such a wave depends on a group of resonant particles whose velocity parallel to the main magnetic field is

*This work was supported principally by the U.S. Atomic Energy Commission under Contract AT(30-1)-3285.

$$v_{||} = \frac{(\omega-\omega_o)}{k}. \tag{2}$$

This is usually explained by observing that these particles see a Doppler-shifted local cyclotron resonance frequency and experience a cyclotron acceleration or deceleration. This is intuitively satisfying, since it presents an image of an efficient energy-transfer mechanism between the waves and the resonant particles. As a matter of fact, this picture is misleading because in the actual case the energy transfer is small, bounded, and periodic. This is easily seen by noting that for these waves propagating principally along the main magnetic field a velocity transformation exists which eliminates the wave electric field and reduces the wave to a periodic spatial magnetic field perturbation.[3] This transformation to the frame moving with the phase velocity of the wave is shown in Fig. XI-29, along with the resonant velocities in the two frames. It is seen that the resonance condition in the laboratory frame reduces to the condition for nonadiabatic motion in the phase frame.

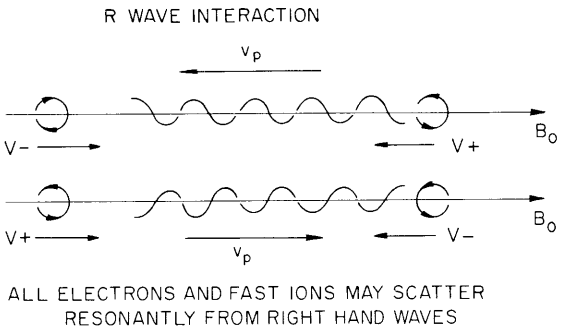

Fig. XI-30. Right-hand wave interaction.

Figure XI-30 represents two oppositely propagating right-hand polarized waves in the phase frame. The spiral line represents the locus of the end of the wave's magnetic field vector. It is also the orbit of a resonant particle. The only possible interaction in this frame is a rotation of the particle's total velocity vector. Consequently, we can represent the laboratory energy transfer in terms of the angular scattering in the variable θ' (defined in Fig. XI-29).

The laboratory energy change is

$$\frac{\Delta W}{W} \approx 2\beta\beta_p\Delta(\cos\theta'), \tag{3}$$

where $\beta = v/c$, and $\beta_p = \omega/kc$. That the energy transfer is small is seen from the fact that $\beta_p \ll 1$. That the energy transfer is periodic is seen from the equations of motion. Roberts and Buchsbaum[4] have shown that

$$W(t) = W(0) + mv_p(v(t)-v(0)), \tag{4}$$

where m is the relativistic mass, and the equation is relativistically correct. Physically, the wave magnetic field accelerates the resonant particles along the main field direction. Thus the resonant particles gain energy only while they are approaching the wave phase velocity. Resonant particles at the phase velocity interact only by virtue of

their perpendicular velocities and are decelerated in the direction of the main field, thereby reversing the energy transfer.

Another way of looking at the interaction is to notice that the ratio of wave magnetic force to wave electric force for the resonant particles is

$$(F_B/F_E) = \left(1 - \frac{\omega_o}{\omega}\right) \gg 1. \tag{5}$$

The wave magnetic field destroys the particle's phase correlation with the wave electric field.

Let us now consider the change in the particle's distribution function because of the passage of one wave. To do so, we first calculate the average change in the perpendicular velocity of a particle interacting with the wave in the phase frame. We can write Newton's equation in the form

$$\frac{dv'_+}{dz} - j\left(\frac{\omega_o}{v'_z}\right) v'_+ = j\omega_+(z), \tag{6}$$

where $v_+ = v_x + jv_y$, and $\omega_+ = \frac{q}{mc}(B_x + jB_y)$. The prime refers to the moving frame (Fig. XI-29).

If we assume that for the great majority of particles the change in z velocity is small, we find the immediate solution

$$\Delta v'_+ = j \int_{-L}^{L} \omega_+(z') \exp\left(-j \frac{\omega_o z'}{v'_z}\right) dz', \tag{7}$$

where $\Delta v'_+$ is the wave induced change in the perpendicular velocity of the particle between L and -L. Since all initial phases are assumed to be present, the average change in this quantity is

$$\left\langle \Delta v'_+ \right\rangle = \frac{1}{2\pi} \int_0^{2\pi} d\phi'_o \, (\Delta v'_+) = 0. \tag{8}$$

The mean-square change

$$\left\langle (\Delta v'_\perp)^2 \right\rangle = \left| \int_{-L}^{L} \omega_+(z') \exp\left(j \frac{\omega_o z'}{v'_z}\right) dz' \right|^2 \tag{9}$$

is finite, however, and constitutes a diffusion coefficient for the particle's perpendicular velocity. Since the total velocity is constant in the phase frame, this can easily be related to the diffusion coefficient in θ'.

Equation 9 can be written in terms of the wave spectra by Fourier-transforming $\omega_+(z)$. We find

$$\left\langle (\Delta v_\perp')^2 \right\rangle = \frac{2}{\pi} \left| \int_{-\infty}^{\infty} dk\, \omega_+^F(k) \frac{\sin\left(k - \frac{\omega_o}{v_z'}\right) L}{\left(k - \frac{\omega_o}{v_z'}\right)} \right|^2 . \tag{10}$$

If L is large, the second factor in the integral oscillates rapidly, and we may replace it by a delta function in $\left(k - \frac{\omega_o}{v_z'}\right)$. Thus we arrive at the final result for the diffusion coefficient as a function of the wave spectra

$$\left\langle (\Delta v_\perp')^2 \right\rangle = \frac{2}{\pi} \left| \omega_+^F \left(\frac{\omega_o}{v_z'} \right) \right|^2 . \tag{11}$$

This coefficient has broad application. The change in the particle's distribution function resulting from the passage of a wave is given by

$$\Delta f = \frac{1}{v_\perp} \frac{\partial}{\partial v_\perp} v_\perp \left\langle \frac{(\Delta v_\perp)^2}{v^2} \right\rangle \frac{\partial}{\partial v_\perp} f. \tag{12}$$

This shows the relaxation effect that the waves produce in the particle distribution. It is interesting to note that Eq. 12 is identical with the result of a quasi-linear calculation by Engel.[2]

We have already shown how the energy transferred in a wave-particle collision can be expressed in terms of the angular scattering in the phase frame. The mean-square energy transfer is

$$\left\langle \left(\frac{\Delta W}{W} \right)^2 \right\rangle = \frac{8}{\pi} \beta^2 \beta_p^2 \left(\frac{v_\perp'}{v_z'} \right)^2 \frac{\left| \omega_+^F \left(\frac{\omega_o}{v_z'} \right) \right|^2}{v^2} . \tag{13}$$

Employing Eq. 13, one can obtain a statistical acceleration mechanism for cosmic rays. One can also obtain a diffusion coefficient for the guiding centers of cosmic ray particles. Assuming that the wave size is small compared with the Larmor radius of the cosmic ray, one can write this coefficient

$$\left\langle (\Delta r_g)^2 \right\rangle \approx r_L \left\langle (\Delta\theta)^2 \right\rangle$$

or

$$\left\langle (\Delta r_g)^2 \right\rangle \approx \frac{v^2}{\omega_o^2} \left(\frac{v_\perp}{v_z} \right)^2 \left\langle \left(\frac{\Delta v_\perp}{v} \right)^2 \right\rangle .$$

Such guiding-center diffusion has been invoked by Davis[5] to explain the isotropy of cosmic rays.

Finally, a number of authors have suggested wave-particle scattering to explain the form of the radiation belts.[6-9] The diffusion coefficients obtained here should also apply to the description of the dynamics of this region.

Report XI-H summarizes an application of the diffusion coefficient to the confinement of particles in static nonadiabatic magnetic fields. By bearing in mind the analogy established above between motion in a static nonadiabatic field and wave-particle interaction, the results given in Sec. XI-H have relevance to the subject of the present report.

J. F. Clarke

References

1. W. P. Allis, S. J. Buchsbaum, and A. Bers, Waves in Anisotropic Plasmas (The M. I. T. Press, Cambridge, Mass., 1963), p. 38.
2. R. Engel, Phys. Fluids 8, 939 (1965).
3. J. F. Clarke, Quarterly Progress Report No. 78, Research Laboratory of Electronics, M. I. T., July 15, 1965, pp. 128-130.
4. L. J. Roberts and S. J. Buchsbaum, Phys. Rev. 135, A381 (1964).
5. L. Davis, Phys. Rev. 101, 351 (1956).
6. D. Wentzel, J. Geophys. Res. 66, 359 (1961).
7. A. J. Dragt, J. Geophys. Res. 66, 1641 (1961).
8. E. N. Parker, J. Geophys. Res. 66, 2673 (1961).
9. J. W. Dungey, Planet Space Sci. II, 591 (1963).

H. NONADIABATIC MAGNETIC TRAPS*

The diffusion coefficient developed in Sec. XI-G can be applied to a study of the relative efficiency of the nonadiabatic traps that are proposed for accumulating a thermonuclear plasma. Three basic types of nonadiabatic fields have been proposed.[1-3] In the complex notation $A+ = A_x + jA_y$, these fields can be represented by

$$\omega_+(z) = \omega_\perp \cos k_o z \qquad -L < z < +L \tag{1a}$$

$$\omega_+(z) = \frac{\omega_\perp}{2} e^{jk_o z} \qquad -L < z < +L \tag{1b}$$

$$\omega_+(z) = \omega_\perp \delta(k_o z), \tag{1c}$$

where k_o satisfies the resonance condition $k_o = \omega_o / v_z^0$ for some resonant velocity v_z^0.

Perturbation (1a) constitutes an axially symmetric field, (1b) a helically symmetric field, and (1c) an impulsive change in the field equivalent to a standing shock wave. This group can be extended by requiring that the resonance condition be satisfied at every point on the particle's orbit. That is, the trap is designed to have a variable wavelength. Each of these variations can be compared in terms of the mean-square step in magnetic moment, which a trapped particle makes on traversing the perturbation. This mean-square step is simply related to the diffusion coefficient given in Sec. XI-G.

Consider the Fourier transforms of the perturbations

$$\omega_+^F(k) = \frac{\omega_\perp}{\sqrt{2\pi}} \left\{ \frac{\sin (k_o - k)L}{(k_o - k)} + \frac{\sin (k_o + k)L}{(k_o + k)} \right\} \tag{2a}$$

$$\omega_+^F(k) = \frac{\omega_\perp}{\sqrt{2\pi}} \frac{\sin (k_o - k)L}{(k_o - k)} \tag{2b}$$

$$\omega_+^F(k) = \frac{1}{\sqrt{2\pi}} \frac{\omega_\perp}{k_o}. \tag{2c}$$

From the diffusion coefficient

$$\left\langle \left(\frac{\Delta v_\perp}{v} \right)^2 \right\rangle = \left| \int_{-\infty}^{+\infty} dk\, \omega_+^F(k) \frac{\sin \left(k - \frac{\omega_o}{v_z} \right) L}{\left(k - \frac{\omega_o}{v_z} \right)} \right|^2 \tag{3}$$

---

*This work was supported principally by the U.S. Atomic Energy Commission under Contract AT(30-1)-3285.

we see that the magnetic moments of the particles will have large changes only when the two factors in the integral overlap appreciably.

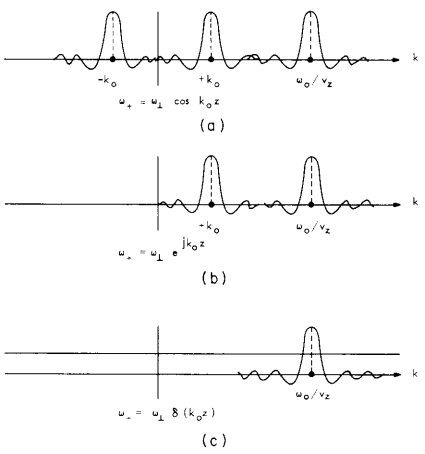

Fig. XI-31. Diffusion coefficient factors in k space.

Figure XI-31 shows graphically the situation for the three perturbations. The initial trapping occurs when $v_z = v_z^0$, and the functions on the positive k axis merge. For trapped particles, there can never be a complete superposition, since some of their initial axial velocity, v_z^0, has been transformed to perpendicular velocity. The net scattering comes from the overlapping of the wings of the peaks. It becomes immediately clear that on the reverse transit through the perturbation, when the ω_o/v_z peak lies on the negative k axis, the rotating perturbation is far superior to the axial symmetric one. Furthermore, the resonant nonadiabatic systems are superior to the nonresonant because in the latter case all velocities interact by the same amount and independently of their direction of motion.

It is also interesting to note the height and breadth of the k_o resonance peaks in Fig. XI-31. The peak height is $\omega_\perp L/2\pi$ and its width is $2\pi/L$. Now, considering the fact that for an untuned system $k_o = 2\pi N/L$, we see that as the system becomes longer and the particle interacts with more periods of the perturbation, the peaks grow in height and become narrower. All of this is in agreement with the physical argument presented by Wingerson, Dupree, and Rose[4] and the numerical calculations of Laing and Robson.[5]

We turn now to a final example of the use of the diffusion coefficient. Wingerson, Dupree, and Rose conclude that a long highly tuned system, in which the perturbation field goes gradually to zero at both ends, would constitute the optimum trap. We can examine such a trap analytically.

Let us consider a trap in which the perturbation wavelength lengthens as z decreases. For simplicity, choose a wave number

$$k_{eff} = k_o + k_1^2 z \tag{4}$$

and a Gaussian envelope to damp the perturbations away from the origin

$$\omega_+(z) = \frac{\omega_\perp}{2} e^{-\gamma^2 z^2} \exp\left[\left(k_o + k_1^2 z\right) z\right] \tag{5}$$

In the light of Sec. XI-G, this is the phase-frame form of a wave packet. The Fourier transform of this function is

$$\omega_+^F(k) = \frac{\omega_\perp}{8} \frac{\exp\left[-\gamma^2 \frac{(k_o-k)^2}{4\left(\gamma^4+k_1^4\right)} + j \frac{k_1^2(k_o-k)^2}{4\left(\gamma^4+k_1^4\right)}\right]}{\left(\gamma^2-jk_1^2\right)^{1/4}}. \tag{6}$$

Since our Gaussian envelope damps the wave, we can take $L \to \infty$ in the integration of the diffusion coefficient. This is equivalent to replacing the sine factor by a delta function. Then the diffusion coefficient reduces to a term proportional to the square of Eq. 6 with k replaced by ω_o/v_z. Note that the damping coefficient and the increasing wavelength coefficient appear in "parallel" in this expression. This illustrates the physical point that both damping and tuning decrease the scatter of nonresonant particles. These particles rotate faster or slower than the perturbation field, and the scattering from each field peak tends to be cancelled by the next peak. Only the last peak scatter has full effect, and the damping reduces this to a low level. Tuning reduces the resonance volume in phase space which is available to particles. In terms of Fig. XI-31, the central peak is narrowed.

To simplify the expression, let us assume that the damping length is large compared as with a wavelength, and that the change in wavelength is small compared with a wavelength. Choosing N wavelengths in our perturbation, we can set

$$\gamma = \frac{k_o}{N} \tag{7a}$$

and

$$k_1 = \frac{k_o}{N}. \tag{7b}$$

The diffusion coefficient simplifies to

$$\left\langle \left(\frac{\Delta v_\perp}{v}\right)^2 \right\rangle = \frac{1}{2} \frac{v_z^{0^2}}{v^2} \left|\left(\frac{\omega_+}{\omega_o}\right)\right|^2 \frac{N^2}{4} \exp\left[-\frac{N^2}{8}\left(1-\frac{v_z^0}{v_z}\right)^2\right]. \tag{8}$$

This expression illustrates the sharpness of the resonance peak.

In conclusion, we find that the physical arguments presented by Wingerson, Dupree, and Rose are in full agreement with calculations performed with the simplified diffusion coefficient derived in Sec. XI-G. An experimental study of this nonadiabatic scattering phenomenon is underway.

J. F. Clarke

References

1. K. D. Sinenikov et al., Soviet Phys. – Tech. Phys. 5, 236 (1960A).

2. R. C. Wingerson, Phys. Rev. Letters 6, 446 (1961).

3. R. C. Wingerson, T. H. Dupree, and D. J. Rose, Phys. Fluids 7, 1475 (1964).

4. E. W. Laing and A. E. Robson, J. Nucl. Energy (Part C, Plasma Phys.) 3, 146 (1961).

I. STUDY OF LASER RADIATION THOMSON-SCATTERED BY AN ELECTRON BEAM*

The present experiment is concerned with the dependence on angle of the frequency of laser light that is Thomson-scattered by a relativistic electron beam. Preliminary calculations had led us to believe that if the laser beam intersects the electron beam at 90° and the angle of observation from the electron beam is 90°, then the relativistic transformations from the laboratory frame of the laser beam to the moving frame of the electron beam and back to the laboratory frame of the observation system would result in a factor of $\gamma^2 \left(\gamma = \left(1 - \frac{v^2}{c^2}\right)^{-1/2}\right)$ in the frequency relation. Thus even when the Doppler shift that is associated with advancing sources (the "normal" shift) is absent, there will be a shift from the laser wavelength of 2 per cent if the beam voltage is 5 kilovolts. An exact examination of the relativistic and normal Doppler transformations shows that, instead of γ^2, the correct factor is unity when the normal shift is zero. Furthermore, the total relativistic transformation from the laboratory frame of the laser to the beam frame and then into the laboratory frame of the observation system is identical to the normal Doppler transformation.

Straightforward calculations of the number of photons scattered by the electron beam, with the Thomson scattering cross section used and the radiation treated as if it were in the form of particles colliding with the electrons and then scattered in all directions, show that in order to have reasonably good statistics the electron beam must have a density greater than 5×10^{10} electrons/cm^3. This value is true for the 50-joule ruby laser used in the experiment when it has been focussed to make a beam of 1 mm diameter. A density such as this corresponds to a beam current of 200 ma at 3 kv if the beam diameter is 1 mm. The number of photons in the incident laser beam is $\approx 10^{20}$, and the number scattered is only 10^5, while the number collected by the observation system is ≈ 500. These 500 photons pass through an interference filter that will pass only radiation whose wavelength lies in a 5Å interval. From there they hit the cathode of a very sensitive photomultiplier and produce photoelectrons with an efficiency of only 2 per cent. With only 10 photoelectrons in each laser shot it is plain that several shots are necessary at each angle and frequency to get good results.

Thus far, an electron gun of the Pierce type has been constructed and after experiencing difficulties in design it eventually evolved to the point where it produces a well-defined beam of about 1 mm in diameter at 200 ma and 3 kv. The gun has a microperveance of 3, and can be operated so that there is no power dissipated in the anode. The

*This work was supported principally by the U.S. Atomic Energy Commission under Contract AT(30-1)-3285.

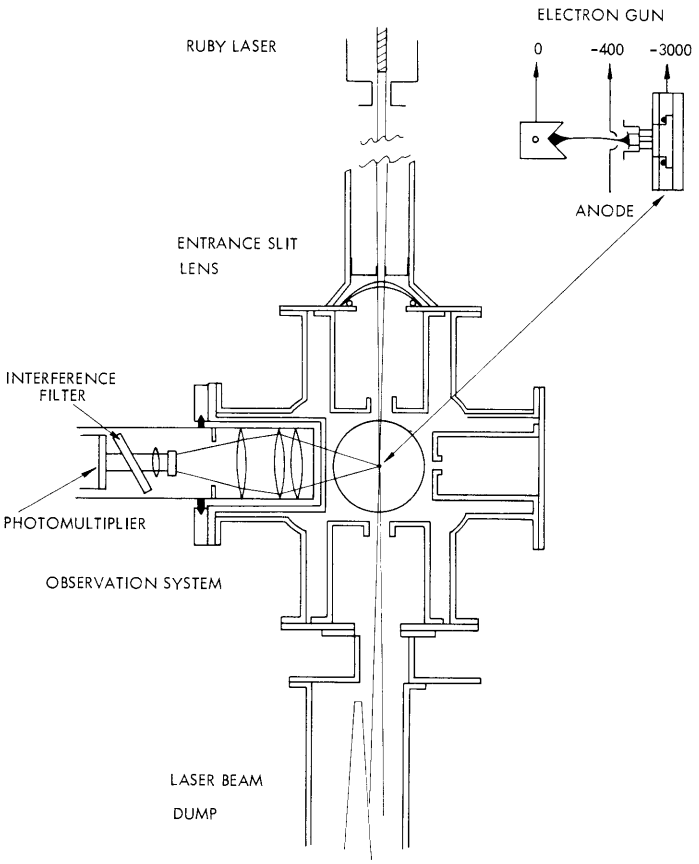

Fig. XI-32. Illustrating the experimental arrangement.

operating pressure is 1×10^{-6} torr, and beam operation is very stable. Also, an observation system was designed and built to cover as large a solid angle as was compatible with frequency spread and vacuum can space requirements. The system can be scanned from an angle of 90° to 70° from the electron beam direction of motion. The arrangement of the various parts of the experiment is shown in Fig. XI-32.

The problem of the reflection of laser light into the observation system has been overcome by the use of special light dumps and aperture stops. The experiment is now under way and it is anticipated that it will be almost completed by December 31, 1965. The electron beam, laser beam, and viewing system have all been operated separately, and trial results are now being obtained and the signal-to-noise in the experiment (the crucial problem here) appears to be satisfactorily low.

M. A. Samis

J. INCOHERENT SCATTERING OF LIGHT FROM A PLASMA. II.*

In Quarterly Progress Report No. 78 (pages 131-135) we reported signal-to-noise calculations for the cooperative scattering effects at small scattering angles of visible laser light from a plasma discharge.[1] Noise measurements of the light emission from the plasma indicated that by using an Argon ion laser of sufficient optical power (tens of watts) one could experimentally undertake the measurement of the weak scattered-light spectrum. Nominal integration times would suffice for signal-to-noise, but the expected spectral width would be small, thereby limiting the attainable resolution. Also, the question of diffracted or otherwise stray laser light at small angles interfering with the scattered, Doppler-shifted wavelength was posed but not answered. Fortunately, this question will no longer arise with the new technique presented in this report.

We wish to report the adoption of a new laser, which was unknown at the time of submitting the last report. The modified experiment will now use an infrared laser developed by Patel of Bell Telephone Laboratories, Inc.[1] It is a nitrogen, carbon-dioxide laser yielding very high power output at 10.6 microns, utilizing closely coupled vibrational levels in N_2 and CO_2. A discharge of 4 kv/m and 50 ma DC, in a tube, ~8 ft long and 1 inch in diameter, with continuous gas flow (CO_2 pressure 0.4 torr, N_2 pressure 2 torr), reported by Patel has yielded up to 16 watts cw of 10.6-micron radiation, coupled out through a hole in one of the end mirrors. The intracavity power was several hundred watts.

An indication of benefits from adopting this laser can be seen from the following discussion. Analogous to the noise calculations of our previous report, we may calculate the equivalent noise powers for an experiment, using 10.6-micron radiation. Note that since the spectral width varies as $\lambda \sin\frac{\theta}{2}$, and that for observation of coherent effects $\frac{\lambda}{4\pi\lambda_D \sin\frac{\theta}{2}} \sim 1$, an increased wavelength (10.6 μ versus 0.5 μ) allows observation at very much larger angles, where λ is the incident wavelength, λ_D is the plasma Debye length, and θ is the scattering angle with respect to incident direction. At 0.5 μ one need work at $\theta = 2°$, leaving no latitude for angular scan, whereas at 10.6 μ one can scan to $\theta = 90°$. Two important features result: (i) a larger solid angle in the detector optics can be used, and (ii) a larger optical bandpass filter can be employed. Note also that detector efficiencies at 10.6 μ versus 0.5 μ (mercury doped germanium and photomultiplier, respectively) are ~100 per cent and ~10 per cent. Since signal-to-noise varies as $\sqrt{\Delta\Omega\Delta\lambda\epsilon}$, where $\Delta\Omega$ is the solid angle, $\Delta\lambda$ is the bandpass, ϵ is the quantum efficiency of the detector, a large increase is to be gained. In fact, the use of 10.6-μ radiation will yield a factor of

*This work was supported principally by the U.S. Atomic Energy Commission under Contract AT(30-1)-3285.

100 increase in signal-to-noise for scattered light versus plasma emission; consequently, the plasma itself will be essentially noise-free for an optical power input of

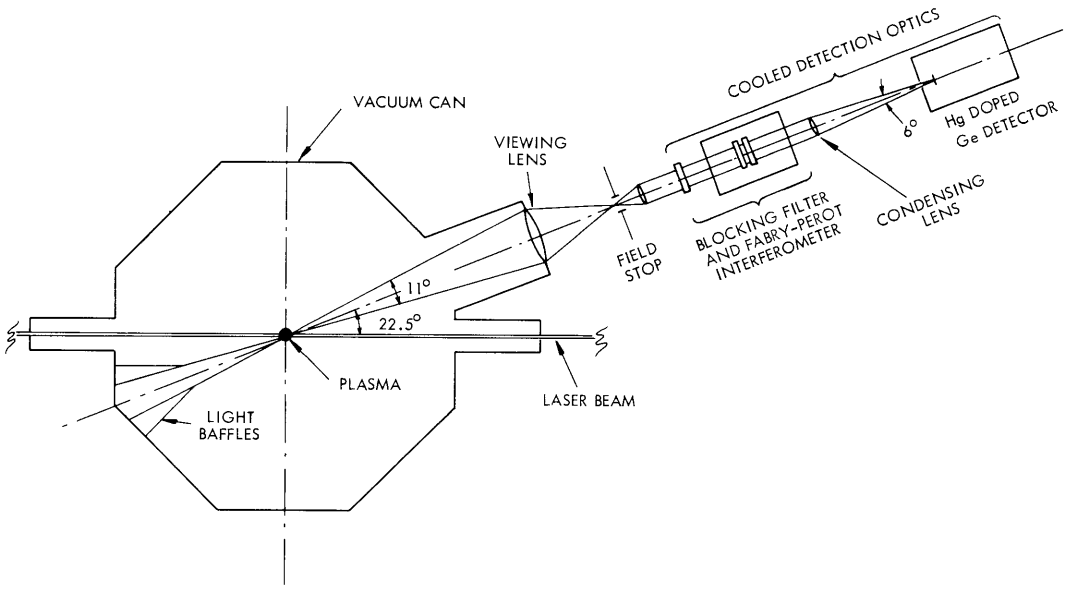

Fig. XI-33. Detection optics.

several watts. With reference to Fig. XI-33, the observational result of scattered radiation at 22.5° (with solid angle $\Delta\Omega = \pi \times 10^{-2}$ and bandpass $\Delta\lambda = 10$ Å) for the hollow-cathode arc plasma ($n_e \sim 10^{14}/cm^3$, $Te \approx 4$ ev) in the worst case, is expected to be 4×10^{-16} Po watts, where Po is incident power. The calculated noise power from the arc, resulting chiefly from Bremsstrahlung is $10^{-15}(\Delta f)^{1/2}$ watts, where Δf is the bandwidth of receiver. Evidently, with several hundred watts incident power the plasma noise can be neglected.

In fact, the experimental noise to be contended with results from fluctuations in thermal black-body radiation at 300°K, the corresponding wavelength maximum occurring at 9.6 μ. Once again, referring to the geometry of the detection optics, we can calculate the noise power at 10.6 μ for the plasma vacuum wall and collection lenses at room temperature, and the remaining optics at dry-ice temperature (cooling results in a significant reduction of noise). The detector (an Hg doped Ge solid-state device) $\approx 10^{-3}$ cm^2 in area, subtending a field of view of 6°, as a result, sees an equivalent noise power from all surfaces of $\sim 10^{-13}(\Delta f)^{1/2}$ watts. Only noise in a 10 Å bandpass from the vacuum wall and collector lenses emerges to the detector, and noise from emission by surfaces following the interferometer is nominally integrated over 10 μ. As a consequence, Po = 250 watts would yield signal-to-noise of unity for a 1-cps receiver bandwidth.

The laser arrangement is shown in Fig. XI-34. A hemispherical mirror mode will be employed with two 10 ft, 1-inch diameter, tubes of optically active media. The plasma

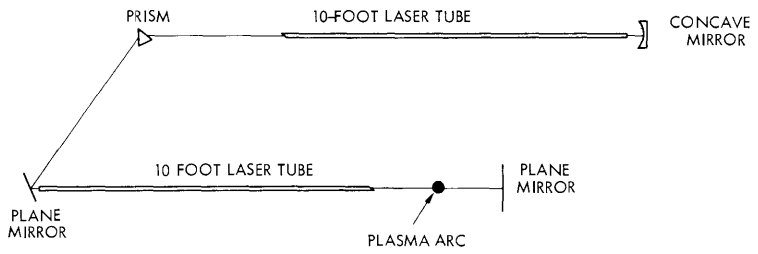

Fig. XI-34. Laser cavity arrangement.

will be placed inside the optical cavity and, with 20 ft of optical gain, the laser power available for scattering should be substantial. A prism is to be used for wavelength isolation; a half-dozen modes separated by 200 Å at 10.6 μ are normally present and are of no consequence to this experiment. The hemispherical mode not only provides efficient use of the laser volume for power generation but also, since the light focuses to a diffraction limited spot on the plane mirror, makes it possible to determine the desired beamwidth at the scattering point merely by positioning the plasma arc back from the plane mirror.

The laser beam will be chopped, and the scattered signal plus noise synchronously detected by using a PARL lock-in amplifier with low-noise preamplifiers. The output will be plotted on an X-Y recorder, with spectral scan achieved by varying the optical path in the Fabry-Perot interferometer (pressurizing with nitrogen). The spectral scan is to be 300 Å in 10 Å steps, to yield good resolution of the enhanced scattering effect that is sought.

A. A. Offenberger

References

1. C. K. N. Patel, Phys. Rev. Letters 13, 617 (1964).